Check for updates

The geodynamics of plume-influenced mid-ocean ridges: insights from the Foundation Segment of the Pacific-Antarctic Ridge

Philipp A. Brandl[1]*, Christoph Beier[2], Karsten M. Haase[3], Felix S. Genske[4], Folkmar Hauff[1], Marcel Regelous[3], Colin W. Devey[1] and Lars H. Rüpke[1]

[1]GEOMAR Helmholtz Centre for Ocean Research Kiel, Kiel, Germany, [2]Department of Geosciences and Geography, Research Programme of Geology and Geophysics (GeoHel), University of Helsinki, Helsinki, Finland, [3]GeoZentrum Nordbayern, Friedrich-Alexander-Universität Erlangen-Nürnberg, Erlangen, Germany, [4]Institut für Mineralogie, Universität Münster, Münster, Germany

The intersection of the Foundation Plume with the Pacific-Antarctic Ridge is a key location in global geodynamics where a mantle plume is approached by and interacting with a fast-spreading mid-ocean ridge. Here, we discuss a comprehensive major and trace element and Sr-Nd-Pb isotope dataset of new and existing samples from the young Foundation Seamount Chain (<5 Ma) and adjacent section of the Pacific-Antarctic Ridge. We use the geochemistry of axial, off-axis and intraplate lavas to map the spatial extent of plume dispersal underneath the ridge as well as the internal zonation of the upwelling plume. We show that the unusual length, increased crustal thickness and occurrence of silicic rocks on the axis of the Foundation Segment are the direct result of plume being tapped by the axial melting zone. We demonstrate that the plume is not homogeneous but shows a HIMU-like (high time-integrated $^{238}U/^{204}Pb$) OIB (Ocean Island Basalt) component characterized by $^{206}Pb/^{204}Pb$ of up to 20.5 in its center and a more EM1-like (Enriched Mantle one) OIB component characterized by low U/Pb and $^{206}Pb/^{204}Pb$ but high Rb/Nb and $^{87}Sr/^{86}Sr$ towards its edges. Plume entrainment leads to a high magma supply rate that fosters the formation of silicic rocks and triggers the lengthening of the segment over time. However, plume dispersal is not symmetric as the geochemical tracers for the OIB component are extending <100 km northwards but >300 km southwards. We relate this to the current plate tectonic framework in which the obliquity between the migrating ridge and the absolute plate motions induces a sub-axial asthenospheric flow that preferentially channels plume material southwards.

KEYWORDS

Foundation, Pacific-Antarctic Ridge, plume-ridge interaction, ridge segmentation, intraplate, mid-ocean ridge, geochemistry

1 Introduction

The composition of lavas erupted along the >65,000 km-long global mid-ocean ridge system is dominated by tholeiitic basalts (MORB) that are the product of adiabatic decompression melting of the depleted upper mantle (e.g., Klein and Langmuir, 1987). Intraplate lavas in contrast are typically more alkaline and carry a unique geochemical signature (i.e., enrichment in incompatible elements and distinct radiogenic isotope ratios) as they are produced by melting material from upwelling, buoyant and geochemically distinct mantle plumes (e.g., Hofmann and White, 1982; Koppers et al., 2021). In many locations globally, mantle plumes and mid-ocean ridges interact producing magmas with mixed geochemical signatures. Iceland represents the prime example of plume-ridge interaction but even in this case, the plume is not centered underneath the ridge axis (Shorttle et al., 2010). When upwelling plume material impinges the lithosphere, it tends to flow laterally towards the ridge axis (younging and thus thinning lithosphere) and produces volcanic lineaments on the overlying plate (Morgan, 1978; Schilling, 1985; Schilling, 1991; Kincaid et al., 1996; Sleep, 1996; Ito et al., 2003; Mittelstaedt and Ito, 2005). At the mid-ocean ridge axis, plume material then spreads along the axis, potentially over hundreds of kilometers, producing an anomalous axial geochemistry and bathymetry (Schilling, 1973; White and Schilling, 1978; Sleep, 1996; Yale and Phipps Morgan, 1998; Ito et al., 2003). The introduction of additional and/or geochemically distinct plume material into a mid-ocean ridge spreading center has important implications for ridge segmentation as it forces ridge segment discontinuities, including overlapping spreading centers (OSCs), to migrate away from the plume (e.g., Briais and Rabinowicz, 2002; Rabinowicz and Briais, 2002). The dynamics of this plume-ridge interaction are thus controlled by the position of the plume relative to the ridge, by plate and ridge motion, and by ridge spreading rate (Ribe et al., 1995; Ito et al., 1996; Ito et al., 1997; 2003; Ribe, 1996; Ribe and Delattre, 1998; Maia et al., 2000). Globally, most plumes interact with spreading centers that are migrating away from the plume and there are only two examples where a plume interacts with an approaching ridge: Louisville (Ribe and Delattre, 1998) and Foundation (this study).

In this contribution we present new and compiled bathymetric and geochemical data from the northern Pacific-Antarctic Ridge (PAR), where a second-order ridge segment approaches the nearby Foundation Plume. This "Foundation Segment" of the PAR is a unique example where a migrating and fast-spreading ridge is influenced by a – based on geophysical constraints (Maia et al., 2000; Maia and Arkani-Hamed, 2002) – supposedly weak plume that is located slightly off the ridge axis. The dense sampling along the Foundation Segment of the PAR allows to use the geochemical plume signal as a chemical tracer injected into the divergent plate boundary's magmatic system. Geological and geochemical mapping of the Foundation Segment and the surrounding area allows us to constrain the composition of the plume as well as the evolving influence of the plume over time and its relevance for ridge segmentation and the axial magmatic system.

2 Materials and methods

2.1 Geological setting

The Foundation Seamount Chain (FSC) in the South Pacific forms a >1,900 km-long, age-progressive line of seamounts that erupted enriched alkaline intraplate lavas and recorded highly variable radiogenic isotope ratios (Devey et al., 1997; Hékinian et al., 1997; 1999; O'Connor et al., 1998; Maia et al., 2001; Stroncik and Devey, 2011). These seamounts mark the track of a moving plate over a near-stationary plume that is upwelling hot mantle material for at least the last 21 Ma but possibly for more than 34 Ma (O'Connor et al., 1998). This longevity together with high ^{3}He/^{4}He (Stroncik and Devey, 2011) and low shear wave velocities (v_s) in the underlying mantle extending to >1,000 km depth (Schmerr et al., 2010) argue for a deep mantle plume origin. Other criteria used by Courtillot et al. (2003) to classify mantle hotspots remain more ambiguous in case of Foundation: a related flood basalt province is missing due to blurring of the seamount trail at ages >34 Ma (O'Connor et al., 1998), and the buoyancy flux of <1 km^3 a^{-1} is weak relative to other plumes even though this may result from the specific geodynamic situation of Foundation (Maia et al., 2000). A detailed discussion whether the Foundation melting anomaly represents a primary plume or secondary hotspot (cf. Courtillot et al., 2003) or whether the hotspot is the surface expression of an underlying mantle plume is beyond the scope of this study. However, three out of five characteristics match the plume criteria after Courtillot et al. (2003) and we thus prefer to use the term "Foundation Plume" throughout this manuscript. The Foundation Plume has been approached by the PAR for more than 10 Ma and about 5 Ma ago the plume started to influence the approaching ridge (O'Connor et al., 1998; 2001; Hékinian et al., 1999; Maia et al., 2000; 2001; Stroncik and Devey, 2011).

The PAR is a westward-migrating, fast-spreading center (~100 mm a^{-1} full spreading rate) that separates the rapidly moving Pacific from the near-stationary Antarctic Plate (Lonsdale, 1994). Spreading is asymmetric with rates up to 55 mm a^{-1} to the east and 45 mm a^{-1} to the west and the PAR is migrating at 28.5 mm a^{-1} to the NW (301°) in the plate motion reference frame of Müller et al. (2022). A single, more than 1,600 km-long first-order ridge segment forms the northern PAR between the Juan Fernandez Microplate in the north and the Ménard Fracture Zone in the south (Lonsdale, 1994; Klingelhoefer et al., 2006). Smaller non-transform offsets including overlapping spreading centers (OSCs) further subdivide the ridge into a total of eight second-order segments. From N to S these are the segment south of the triple junction with the Juan Fernandez Microplate (TJ Segment) and the Foundation Segment (this study), and the N6 to N1 segments (Klingelhoefer et al., 2006; ascending numbers from S to N: Hamelin et al., 2010). In this contribution, we focus on the TJ, Foundation, N5 and N6 segments that make up the northernmost section of the PAR from 35°30'S to ~44°S (Figure 1). Particular attention is drawn to the Foundation Segment, as it represents an unusually long (~550 km) second-order ridge segment that is bound at both ends by southward-migrating OSCs at 36.5°S and 41.5°S (Figure 1; Lonsdale, 1994). The rate of OSC migration is slower in the north (~20 km Ma^{-1}) than in the south (45–60 km Ma^{-1}), which results in a lengthening of the segment over time (Lonsdale, 1994).
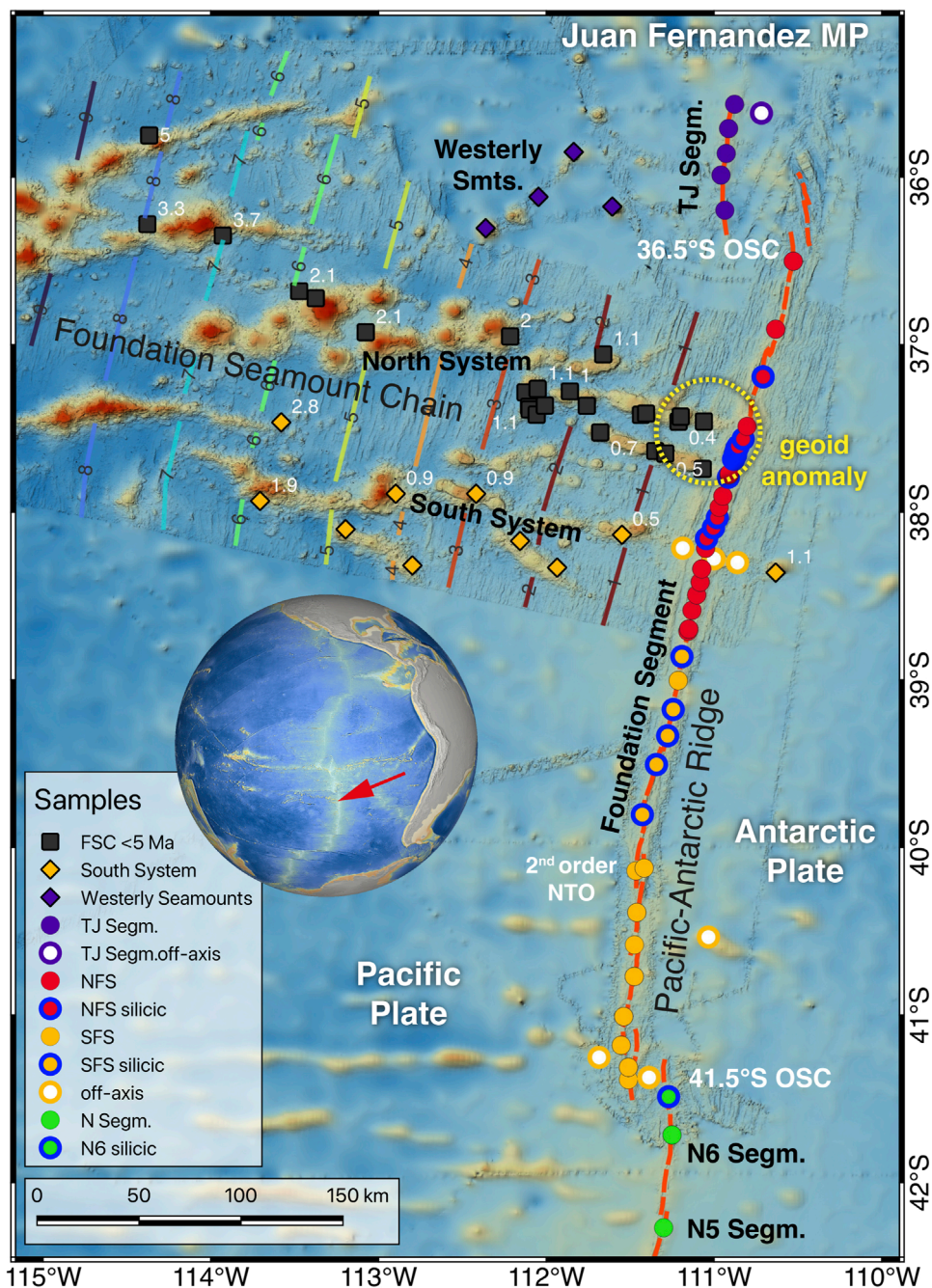
FIGURE 1
Map of the intersection of Foundation Seamount Chain and the Pacific-Antarctic Ridge south of the Juan Fernandez Microplate (MP) to 42°S. The yellow dashed circle illustrates the location of the 0.1 m-geoid anomaly after Maia et al. (2001). Bathymetry enhanced by slope and hill shading. Colored lines on "Hotline" bathymetry illustrate isochrons with ages in Ma after (Maia et al., 2005). White numbers give radiometric seamount ages (in Ma) after (O'Connor et al., 1998; O'Connor et al., 2001). Bathymetry: GMRT v4.2 (Ryan et al., 2009), RV L'Atalante cruise "Hotline" (gridded at 130 m), and RV Sonne cruises SO157 and SO213 (gridded at 100 m). FSC – Foundation Seamount Chain, JFMP – Juan Fernandez Micro Plate, NFS – Northern Foundation Segment, NTO – Non-Transform Offset, OSC – Overlapping Spreading Center, SFS – Southern Foundation Segment, TJ Segm. – Triple Junction Segment, N Segm. – N Segments after Klingelhoefer et al. (2006).

The Foundation Segment is magmatically inflated as evident from its morphology with axial domes along most of its length, a 200–300 m shallower axis compared to the neighboring PAR segments, and crustal thickening by ~1.5 km (Maia et al., 2000) relative to normal oceanic crust. Tholeiitic basalts are the dominant lithology along the Foundation Segment but highly differentiated rocks including basaltic andesites, andesites and dacites are erupted alongside (Hékinian et al., 1997; 1999; Stoffers et al., 2002; Haase et al., 2005; Freund et al., 2013; Figure 2). In this contribution, we use the term "silicic lavas" to refer to this suite of differentiated
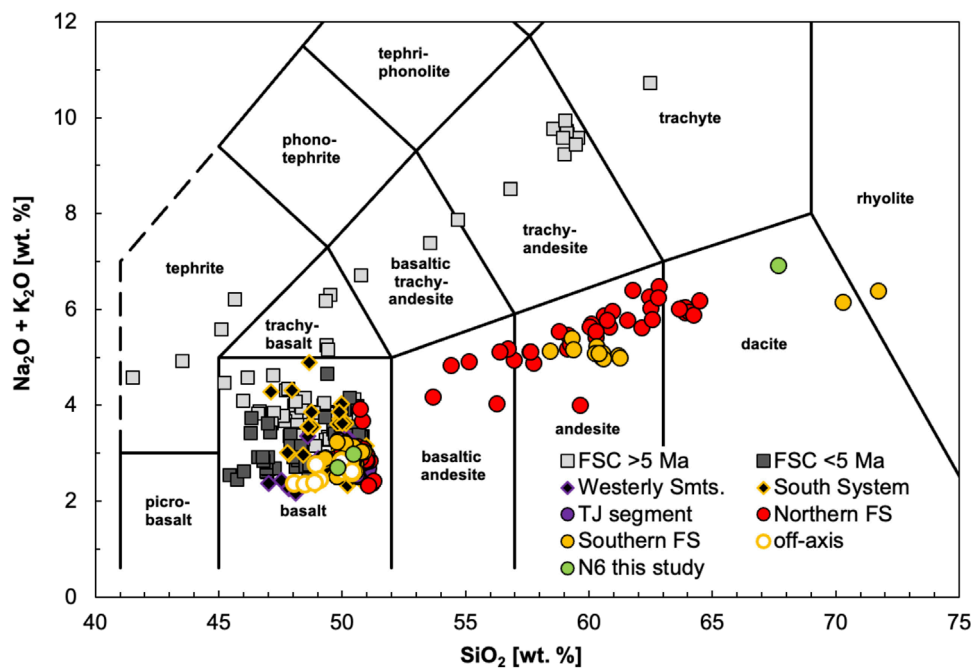
FIGURE 2
Total alkali (Na$_2$O+K$_2$O) versus silica (SiO$_2$) diagram after Le Maitre et al. (2002). All data are recalculated to a volatile-free basis and normalized to a total of 100. Data listed in Supplementary Table S3. Smts. – Seamounts, FS – Foundation Segment, other abbreviations as in Figure 1.

rock compositions. These silicic lavas are likely to originate from a combined process of extensive fractional crystallization and either assimilation of hydrothermally altered oceanic crust (Haase et al., 2005; Freund et al., 2013) or direct assimilation of a hydrothermal brine (Kendrick et al., 2017). Consistently, at least six distinct hydrothermal vents sites are known from the PAR close to its intersection with the FSC. The occurrence of high Sr and Pb isotope signatures and incompatible element enriched lava compositions along the ridge axis [both relative to normal mid-ocean ridge basalt (N-MORB)] has been interpreted as a plume flux into the PAR axis (Devey et al., 1997; Hékinian et al., 1997; Maia et al., 2000; Haase et al., 2005), however, the seamount lavas are both more enriched and depleted than lavas from the PAR (Stroncik and Devey, 2011). The presence of intraplate compositions that are more depleted than the neighbouring PAR along with the distribution of He and Ne noble gas signatures has led Stroncik and Devey (2011) to conclude that deep, primitive plume-sourced magmas are preferentially channelled and erupted along the spreading axis while the remaining residual mantle is melting underneath near-axis seamounts but not along the axis itself.

Currently, the center of the Foundation Plume is located only 20–35 km west of the PAR axis at ~37.5°S as inferred from a ~100 km broad geoid anomaly (0.10 m threshold, 0.15 m maximum: Maia et al., 2000; Maia et al., 2001; Maia et al., 2005; Figure 1). This very short distance between plume center and ridge, and the fast-spreading rate of the PAR diminishes the geophysical signals of the plume as these are a function of plume-ridge distance and spreading rate (e.g., Schilling, 1991; Ribe and Delattre, 1998; Maia et al., 2000). Estimates on plume volume flux (<1.0 km^3 a^{-1}) and mantle excess

temperature (~20 K) are thus low compared to other plumes (e.g., Galápagos, Sala y Gómez, Louisville), which let Maia et al. (2000) conclude that Foundation is a rather weak plume. The lack of present or former islands (with the possible exception of Darwin Seamount at 121.55°W) along the FSC adds further support for their conclusion.

The morphological expression of intraplate volcanism also changed when the plume started to interact with the ridge: prior to ~5 Ma (or west of 115°W), edifices of the FSC are composed of individual large volcanoes typical for intraplate hotspot volcanism, whereas younger edifices (east of 115°W) form elongated volcanoes suggestive of fissure eruptions and volcanic ridges (Devey et al., 1997; Hékinian et al., 1997; Maia et al., 2001). These ridges form partly *en echelon* and by coeval volcanism with a ~1 Ma periodicity (O'Connor et al., 2001). Near the PAR, intraplate volcanism associated with the Foundation Plume results in the formation of two distinct volcanic lines at a distance of >50 km, the North and the South System (Figure 1). The latter exists for <5 Ma and is likely formed by plate flexure at the margins of the geoid anomaly that allowed melts to percolate through the cracked lithosphere (Maia and Arkani-Hamed, 2002). The North System, in contrast, forms in direct extrapolation of the FSC towards younger ages and represents the most recent intraplate volcanic surface expression of the Foundation Plume (Maia et al., 2001). The North and South System both show a decreasing age difference between their age of formation and the underlying oceanic basement formed at the PAR that reflects the closing distance between the stationary plume and approaching ridge (Maia et al., 2005). When plume-ridge interaction started, seamounts were forming on ~4.5 Ma-old crust and >200 km away from the ridge; The youngest (0–0.5 Ma)

seamounts in contrast form only 20–30 km off the ridge axis (Maia et al., 2005; Figure 1).

2.2 Geochemical analyses and database compilation

This study integrates published and unpublished data into a single, internally consistent dataset of the FSC and the northern PAR. All samples were collected by dredging and wax coring along the FSC and the neovolcanic zone of the PAR between 36°S and 41.5°S during expeditions SO100 (1995), SO157 (2001) and SO213 (2010/2011; new samples) of the German RV *Sonne* and during the HOTLINE cruise of the French RV *L'Atalante* (1997). All samples are unaltered and either contain volcanic glass or are whole rock samples.

Glass samples were crushed, handpicked, and washed with deionized water prior to geochemical analyses. Whole rock samples were cut (to remove oxidized surfaces), rinsed with deionized water in an ultrasonic bath, crushed in a steel jaw breaker and powdered in an agate mill. Major and minor element compositions of SO100 and SO157, and HOTLINE glass samples were analyzed using the JEOL JXA-8900 electron microprobe at the CAU Kiel following the methods and conditions outlined by Fretzdorff et al. (2004) during the same period. The major element contents of the new SO213 glasses were determined using the JEOL JXA-8200 electron microprobe at the GeoZentrum Nordbayern, FAU Erlangen-Nürnberg, and using 15 kV acceleration voltage, 15 nA beam current and a defocused beam diameter (10 μm). Counting times were set to 20 s and 10 s for peaks and backgrounds for all elements, and 40 and 20 s for Cl. The data quality was checked by continuously monitoring the VG-2 and VG A-99 reference glasses (see Brandl et al., 2013). Major element compositions of SO213 whole rock samples were analyzed by X-ray fluorescence on a Spectro XEPOS PLUS at the GeoZentrum Nordbayern in Erlangen and details on the analytical procedure are included in Haase et al. (2016). Results are reported in Supplementary Table S1 of the Supplementary Material.

Trace elements of SO100, SO157 and HOTLINE samples were determined on an Agilent 7500c/s quadrupole Inductively Coupled Plasma Mass Spectrometer (ICPMS) at the CAU Kiel following the procedures outlined in Garbe-Schönberg (1993). Repeated analyses of international rock standards BHVO-2 and BIR-1 yield a precision and accuracy better than 5% and 8% (2σ), respectively (see Freund et al., 2013). Trace element compositions of SO213 samples have been determined using the Thermo X-Series 2 quadrupole ICPMS at the GeoZentrum Nordbayern following the procedures described in Freund et al. (2013). Accuracy and precision were determined by repeated analysis of international rock standards and are within 2%–5% (2σ), except for Sc, Cs, Th and Ta (5%–8%; Freund et al., 2013).
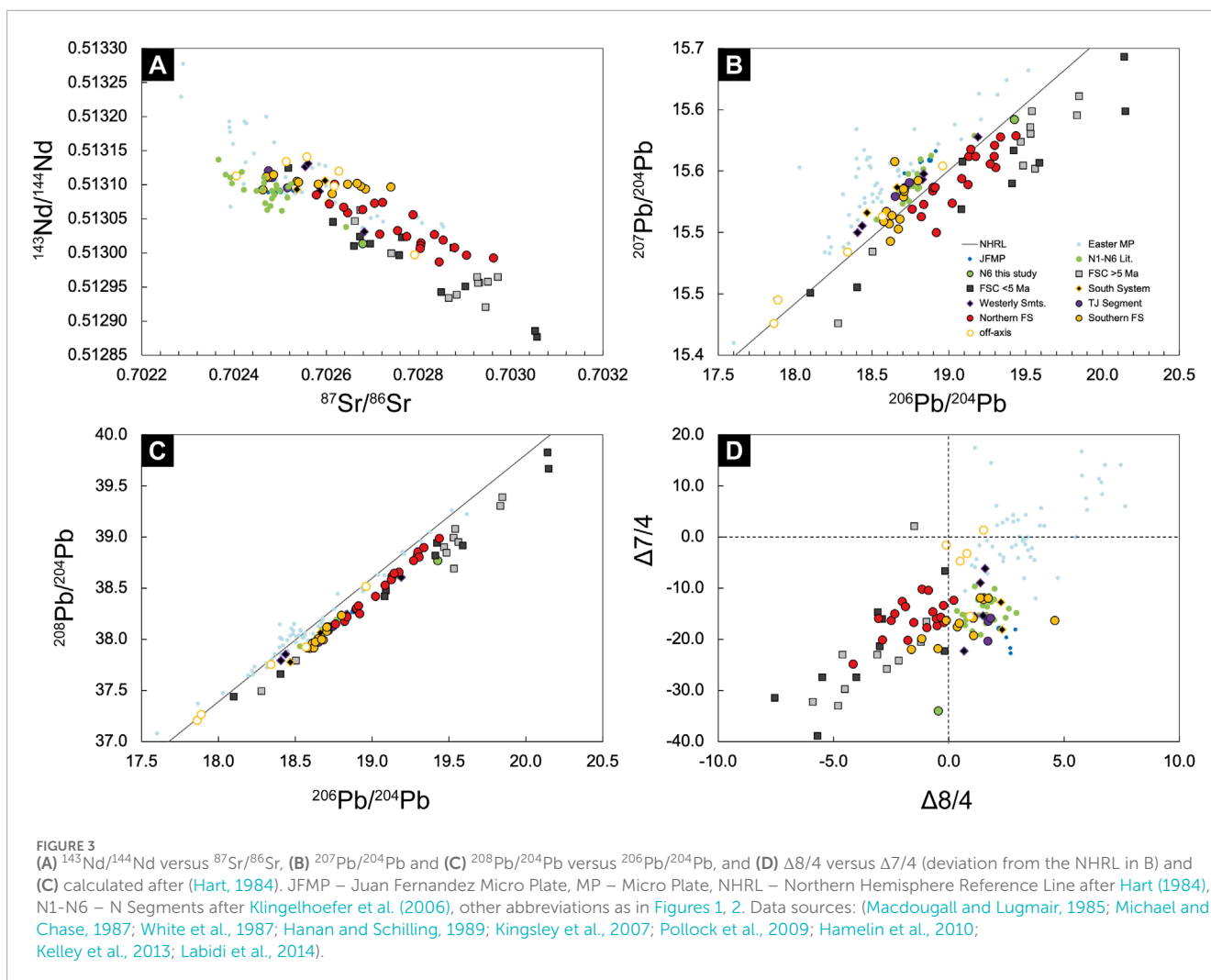
Radiogenic Sr-Nd-Pb isotopes were analysed for a subset of SO100, SO157, SO213, and HOTLINE samples. Previously unreleased Sr-Nd-Pb data of C.W. Devey follow the analytical procedure outlined in Stroncik and Devey (2011), and those of K.M. Haase follow the analytical routine outlined in Haase et al. (2005). Those data are marked red in the integrated dataset reported in Supplementary Table S2. More recently, Sr-Nd isotope

data on selected SO100 and SO157 samples were presented by Freund et al. (2013). Here we present new Sr-Nd and Pb double spike isotope data for the SO213 samples acquired by thermal ionization mass spectrometry (TIMS) using the Thermo Scientific TRITON and Finnigan MAT 262 at GEOMAR in Kiel. The dissolution and separation techniques are described in detail in Hoernle et al. (2011). The 2σ errors reported throughout this contribution represent the twofold standard deviation (2SD) of repeated measurements. The values of reference material measured along with the samples are in good agreement with published and internationally accepted values: SRM NBS-987 (n = 14) yields $^{87}Sr/^{86}Sr$ = 0.710250 (±0.000009, 2σ), La Jolla (n = 12) yields $^{143}Nd/^{144}Nd$ = 0.511850 (±0.000005, 2σ) and double spike corrected SRM NBS-981 (n = 48) values yield $^{206}Pb/^{204}Pb$ = 16.9408 (±0.0013, 2σ), $^{207}Pb/^{204}Pb$ 15.4981 (±0.0014, 2σ) and $^{208}Pb/^{204}Pb$ = 36.7225 (±0.0037, 2σ). Repeat analysis of SO213-9VSRA separate dissolutions are within 2σ of the reference materials and thus analytical errors are smaller than the symbol size in any of the figures. New samples from SO213 are presented in Supplementary Table S1.

The various datasets have then been merged into a single, comprehensive database that has been thoroughly evaluated for potential interlaboratory bias. For unpublished older data and publications without given standard deviations, the values of Kokfelt et al. (2006) were applied because the corresponding FSC-PAR data was generated on the Finnigan MAT 262 at GEOMAR Kiel during the same period. In summary, the older data is reported relative to $^{87}Sr/^{86}Sr$ = 0.710250 for SRM NBS-987 with a max. 2SD of ±0.000025. Likewise, $^{143}Nd/^{144}Nd$ is reported relative to 0.511854 with a max. 2SD of ±0.000009. The older Pb data applied external mass bias correction relative to the SRM NBS-981 values of Todt et al. (1984, 1996) and unspiked SRM NBS-981 reproduces at ±0.006, ±0.007 and ±0.022 for $^{206}Pb/^{204}Pb$, $^{207}Pb/^{204}Pb$, $^{208}Pb/^{204}Pb$, respectively. In conclusion, values for Sr-Nd-Pb reference materials are similar throughout the entire data set and overlap within 2SD (Supplementary Table S3). The higher 2SD's of the older data sets are negligible with respect to the observed isotopic variations and we thus consider our constraints as highly robust in the light of a dataset acquired over 20 years on different instruments and using different analytical routines. The compilation of all samples from the study area including location, water depth, type of material and results from geochemical analyses is provided in Supplementary Table S2 (integrated dataset).

3 Results

Lavas erupted along the FSC prior to 5 Ma are alkaline and range in composition from alkali basalt through to trachyte with subordinate basanite and subalkaline basalt (Figure 2). In contrast, lavas that were erupted intraplate but after plume-ridge interaction started 5 Ma ago (i.e., at near-ridge seamounts) are exclusively basaltic, predominantly subalkaline, and partially overlap with local MORB in terms of their total alkali vs. silica content (Figure 2). All FSC lavas are characterized by their unique incompatible trace element and radiogenic isotope signature that is similar to other Ocean Island Basalts (OIBs). This OIB signature is characterized by elevated incompatible element ratios including K/Ti, Nb/Zr,
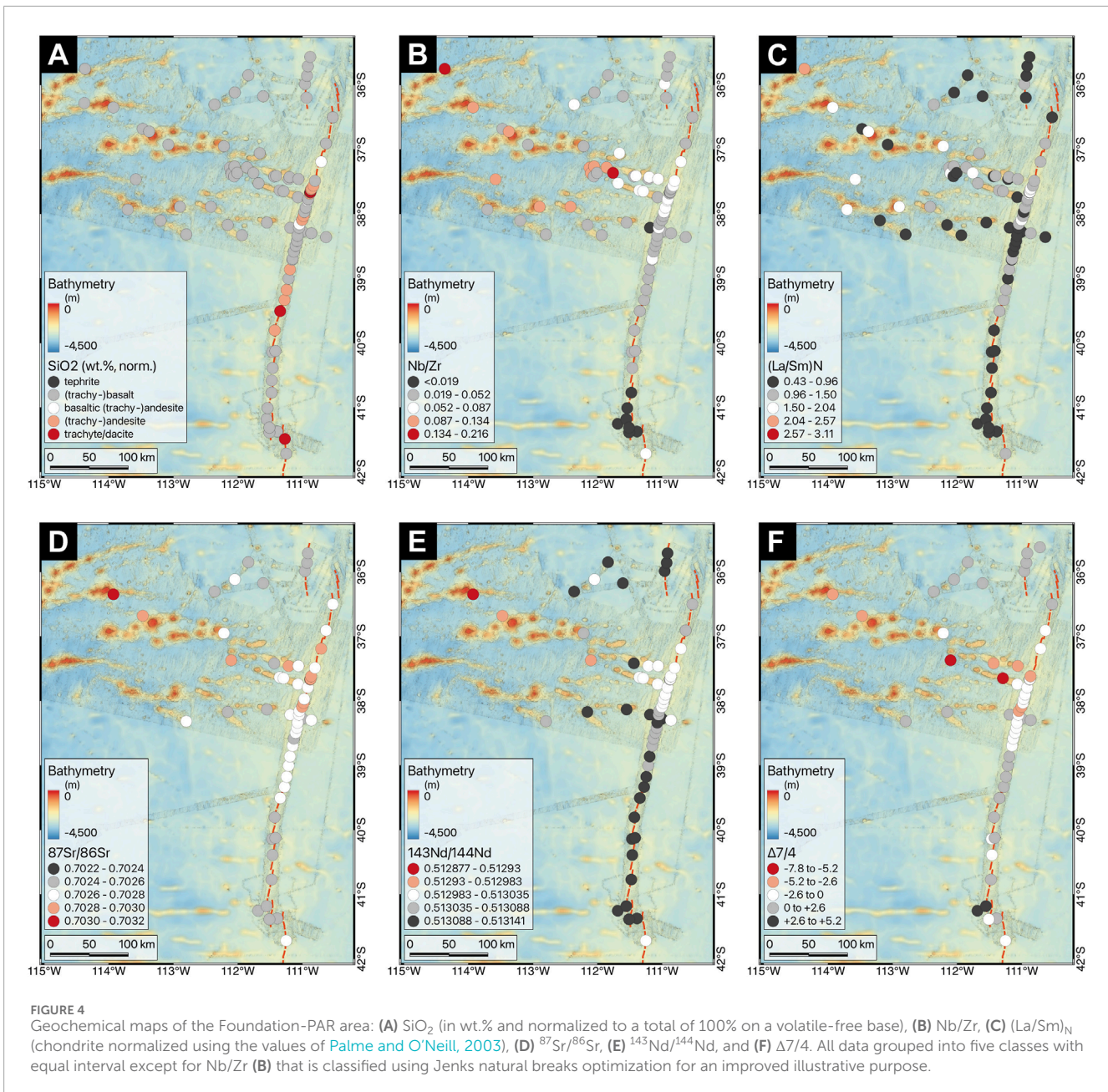
FIGURE 3
(A) $^{143}Nd/^{144}Nd$ versus $^{87}Sr/^{86}Sr$, **(B)** $^{207}Pb/^{204}Pb$ and **(C)** $^{208}Pb/^{204}Pb$ versus $^{206}Pb/^{204}Pb$, and **(D)** Δ8/4 versus Δ7/4 (deviation from the NHRL in B) and **(C)** calculated after (Hart, 1984). JFMP – Juan Fernandez Micro Plate, MP – Micro Plate, NHRL – Northern Hemisphere Reference Line after Hart (1984), N1–N6 – N Segments after Klingelhoefer et al. (2006), other abbreviations as in Figures 1, 2. Data sources: (Macdougall and Lugmair, 1985; Michael and Chase, 1987; White et al., 1987; Hanan and Schilling, 1989; Kingsley et al., 2007; Pollock et al., 2009; Hamelin et al., 2010; Kelley et al., 2013; Labidi et al., 2014).

chondrite-normalized Ce/Yb ($(Ce/Yb)_N$) and La/Sm ($(La/Sm)_N$), as well as enriched Sr, Nd and Pb isotope ratios (Figure 3). All FSC lavas have negative Δ7/4 and Δ8/4 (deviation from the Northern Hemisphere Reference Line of Hart (1984) in $^{206}Pb/^{204}Pb$ versus $^{207}Pb/^{204}Pb$ and $^{206}Pb/^{204}Pb$ versus $^{208}Pb/^{204}Pb$, respectively; Figure 3D). However, some FSC lavas also record more depleted compositions relative to the adjacent portion of the PAR between 36°N and 38°N and MORB in general. These depleted FSC lavas are characterized by particularly unradiogenic $^{206}Pb/^{204}Pb$ of <18.5 (cf. Stroncik and Devey, 2011).

Recent lavas from the Foundation Segment of the PAR show a bimodal distribution in SiO_2 and MgO and can thus be divided into a tholeiitic MORB suite (SiO_2 = 50 ± 2 wt.%, MgO >5.9 wt.%) and a more evolved suite ranging from basaltic andesite to rhyodacite (SiO_2 = 53.6–71.7 wt.%; Figure 2) but also including some low-Mg, Fe-Ti-rich basalts (SiO_2 <52 wt.%; MgO <4.0 wt.%, TiO_2 >3.5 wt.%, FeO^t ~16.5 wt.%). This suite of more differentiated, "silicic" rocks (SiO_2 >52 wt.%) occurs at three distinct locations: at the intersection of the PAR with the North and South System of the Foundation Plume where they are associated with basalts, and further south between 38.8° and 40.0°S, where sampled lavas are silicic in composition (Figures 1, 4). Basalts erupted along the Foundation

Segment can be subdivided into normal (N-)MORB (K/Ti <0.09), transitional (T-)MORB (K/Ti = 0.09–0.15), and enriched (E-)MORB (K/Ti >0.15; K_2O >0.20 wt.%; cf. Cushman et al., 2004). Normal MORBs occur mainly along the Foundation Segment south of 40°S (with no basalts recovered between 39° and 40°S) and the northern TJ Segment. Transitional MORBs are sampled all along the Foundation Segment between the northern OSC and 39.0°S and around the 40.2°S non-transform offset (Figure 1). Enriched MORBs are restricted to two spatially closely related sampling sites at the intersection of the PAR with the North Ridge (SO157-2DS and -17DS), and additional occurrences on the TJ Segment (SO213-4VSR) to the north and the N6 Segment (SO157-46DS) to the south (Figure 4). However, all axial lavas from the Foundation Segment record higher contents (e.g., Rb, Nb, Ba, light rare earth elements (REE)) and ratios of incompatible elements (e.g., $(La/Sm)_N$, Nb/Zr), and are distinct in their radiogenic Sr, Nd and Pb isotope ratios relative to MORB of the neighboring segments (Figure 3).

All regional MORB (Juan Fernandez Microplate, and TJ, Foundation, N1-N6 segments of the PAR) have negative Δ8/4 like the FSC lavas but differ in Δ7/4, with samples from the microplate, and TJ and N1-N6 segments showing exclusively positive Δ7/4 and those of the Foundation Segment recording positive and negative

FIGURE 4
Geochemical maps of the Foundation-PAR area: **(A)** SiO$_2$ (in wt.% and normalized to a total of 100% on a volatile-free base), **(B)** Nb/Zr, **(C)** (La/Sm)$_N$ (chondrite normalized using the values of Palme and O'Neill, 2003), **(D)** ^{87}Sr/^{86}Sr, **(E)** ^{143}Nd/^{144}Nd, and **(F)** Δ7/4. All data grouped into five classes with equal interval except for Nb/Zr **(B)** that is classified using Jenks natural breaks optimization for an improved illustrative purpose.

Δ7/4 values (Figure 3D). This difference is also observed in εNd (calculated using the ^{143}Nd/^{144}Nd value for chondritic uniform reservoir of Goldstein et al. (1984)) with values of +8.5 to +9.5 for the ambient MORB mantle but values as low as +4.6 for the FSC and +6.8 for lavas of the Foundation Segment at the plume-ridge intersection.

4 Discussion

4.1 Plume-ridge interaction in time and space

Several studies have addressed the geochemical and morphological changes along the FSC that result from the decreasing distance between the Foundation Plume and the PAR (Devey et al., 1997; Hékinian et al., 1997; 1999; Maia et al., 2001; 2005; Stroncik and Devey, 2011). Hence, we will only discuss the main features relevant to this study. While light REE enrichment and heavy REE depletion (due to deep partial plume melting in the stability field of garnet peridotite) is a ubiquitous feature of OIB lavas, their specific Sr-Nd-(Hf)-Pb isotope signature is a function of involvement of distinct mantle endmembers (e.g., Stracke et al., 2005). Where plumes interact with mid-ocean ridges, the OIB component thus can be traced by their distinct incompatible trace element and radiogenic isotope signature (e.g., Schilling, 1991; Haase et al., 1997; Janney et al., 2000). With decreasing distance between the plume and the mid-ocean ridge, intraplate lavas become less enriched as a result of a thinner lithospheric lid and thus a shallower final depth of melting and greater contribution from the depleted upper mantle

(e.g., Kokfelt et al., 2006; Beier et al., 2011; Niu et al., 2011). These effects are also observed along the FSC: 1) the volcano morphology changes from isolated large edifices to narrow oblique ridges (e.g., Hékinian et al., 1997; Maia et al., 2000); 2) FSC lavas west of 115°W are alkaline whereas those east of 115° are transitional between alkaline and tholeiitic (Figure 2); 3) the most prominent light REE enrichment, highest Sr (with the exception of PAR silicic rocks) and Pb, but lowest Nd isotope ratios are recorded in the older FSC lavas (west of 115°W); younger FSC lavas are highly variable and record compositions between OIB and MORB.

Since 1.1 Ma, the North System of the FSC forms volcanic ridges with an orientation subparallel to spreading direction and the distinct samples record a large geochemical heterogeneity (cf. Hékinian et al., 1999; Maia et al., 2001). This change in morphology is thought to reflect the onset of plume material being diverted to the ridge axis (Maia et al., 2000; Maia and Arkani-Hamed, 2002). Along the individual volcanic centres of the North Ridge, erupted lavas record a wide range in $^{143}Nd/^{144}Nd$ and $^{206}Pb/^{204}Pb$ of 0.51294 to 0.51313 and 18.29 to 20.23, respectively. However, their calculated average composition is 0.51302 (±0.00005, n = 7) and 19.22 (±0.50, n = 18) for $^{143}Nd/^{144}Nd$ and $^{206}Pb/^{204}Pb$, and therefore matches the composition of axial PAR lavas ($^{143}Nd/^{144}Nd$ of 0.51301 ± 0.00001, n = 7; $^{206}Pb/^{204}Pb$ of 19.23 ±0.11, n = 8) erupted along the corresponding stretch of the Foundation Segment (37.19–37.67°S). Near 37.5°S, PAR MORBs thus record the homogenised radiogenic isotope composition of the near-ridge intraplate lavas with a five times larger variability. While the North System is more likely to tap the true compositional heterogeneity of the source (depleted MORB mantle, enriched OIB source), melt mixing and efficient homogenisation in the axial magma system produces the narrow compositional range recorded at the ridge. This also implies that near-ridge seamounts and the PAR axis at the plume-ridge intersection may be fed by similar mantle sources. We interpret this as direct evidence for both, the channelling of plume material into the axial melting zone (cf. Schilling, 1991; Stroncik and Devey, 2011), and the homogenizing effects of the axial magma system (e.g., Maclennan, 2008; Rubin et al., 2009; Shorttle et al., 2016).

In contrast, samples collected along the South System (Planck and Rutherford seamounts) and off-axis from the PAR at the corresponding latitude record incompatible trace element and radiogenic isotope compositions that are similar to, or more depleted (e.g., $^{206}Pb/^{204}Pb$ <18.50, $^{143}Nd/^{144}Nd$ >0.51307) than axial samples at this latitude (38.16–38.42°S; Figure 5). The difference between axial and off-axis samples may be best explained by the contribution of the enriched plume component restricted to the ridge axis. Samples with similar isotope characteristics are also sampled at the "Westerly Seamounts" (Figure 1) and at the Ohm and Becquèrel seamounts. All of these samples are characterized by higher Rb/Nb compared to most other samples from the Foundation Segment of the PAR or the FSC. The more depleted composition of these off-axis and intraplate samples results from melting of a mantle source that lacks the HIMU-type plume component and thus may be composed of either a second plume component and/or a residual mantle component. The nature of this mantle source will be discussed further below.

Along the FSC we observe the temporal evolution of plume-ridge interaction since 5 Ma. Sampling recent lavas from the Foundation Segment of the PAR axis allows to map the current spatial extent of this interaction. Generally, the least differentiated MORBs are consistent with other ridge basalts derived from rather high degrees of partial melting (e.g., high SiO_2, low TiO_2 and K_2O, low Na_2O/TiO_2) of a peridotitic mantle source at relatively low pressure (<2 GPa; cf. Jackson and Dasgupta, 2008), similar to what is expected for a mid-ocean ridge setting. However, T- and E-MORBs erupt along the Foundation Segment and incompatible trace element contents and ratios (e.g., Nb/Zr, $(La/Sm)_N$, $(Ce/Yb)_N$, U/Pb) as well as radiogenic Sr-Nd-Pb isotope compositions are enriched relative to normal MORB. The geochemically most enriched MORBs (characterized by e.g., highest $(La/Sm)_N$, lowest Δ7/4) erupt near the center of the geoid anomaly at 37.5°S where the Foundation Plume and PAR are closest (Figures 4, 5). Northwards, the enriched geochemical signature drops off quickly (within <100 km) so that axial basalts erupted along the TJ Segment between the 36.5°S OSC and the triple junction with the Juan Fernández Microplate record ambient N-MORB values (Figures 5C–E). Southwards of 37.5°S, Nd and Pb isotope ratios of axial lavas remain more enriched than ambient MORB over a distance of ~150 km (Figures 5D,E). Similarly, contents (e.g., Rb, Nb, Ba, light REE) and ratios of incompatible elements (e.g., K/Ti, La/Sm, Nb/Zr), and $^{87}Sr/^{86}Sr$ are much higher close to the center of plume-ridge interaction and are gradually decreasing southwards. Their values remain elevated relative to ambient MORB over more than 300 km of axial length which is about two times the distance from the plume center compared to observations from Nd and Pb isotopes (Figure 5). Between 40.0 and 41.0°S, axial basalts record $^{206}Pb/^{204}Pb$ values lower than the ambient MORB mantle (Figure 5E). At the same time, these basalts show low U/Pb but slightly elevated Rb/Nb. Only south of the 41.5°S OSC, axial PAR lavas are indistinguishable from ambient MORB with respect to both incompatible element and radiogenic (Sr-Nd-Pb) isotope ratios (Figure 5).

For our goal of mapping out the spatial extent of plume dispersal along the ridge axis, the stretch between 38.8 and 40.0°S is critical as incompatible trace elements and radiogenic isotope ratios show a distinct behavior with respect to a potential plume influence. However, as all but a single sample are highly differentiated rocks, it is important to evaluate the role of crustal processes in altering trace element and isotopic tracers prior to mapping the geochemical domains.

4.2 Formation of silicic lavas in the context of plume-ridge interaction

Basaltic andesites, andesites, dacites and some rhyodacites erupt at three distinct locations along an anomalously shallow portion of the PAR ridge axis with thicker crust (Hékinian et al., 1999; Maia et al., 2000; Stoffers et al., 2002; Haase et al., 2005; Freund et al., 2013). Previous studies have focused on these silicic rocks and explain their formation through extensive fractional crystallization in relatively hot crust coupled to assimilation of hydrothermally altered oceanic crust driven by rift propagation into colder oceanic crust (Haase et al., 2005; Freund et al., 2013). The presence of geochemically enriched lavas along the Foundation Segment of the PAR led to the conclusion that the inflow of plume
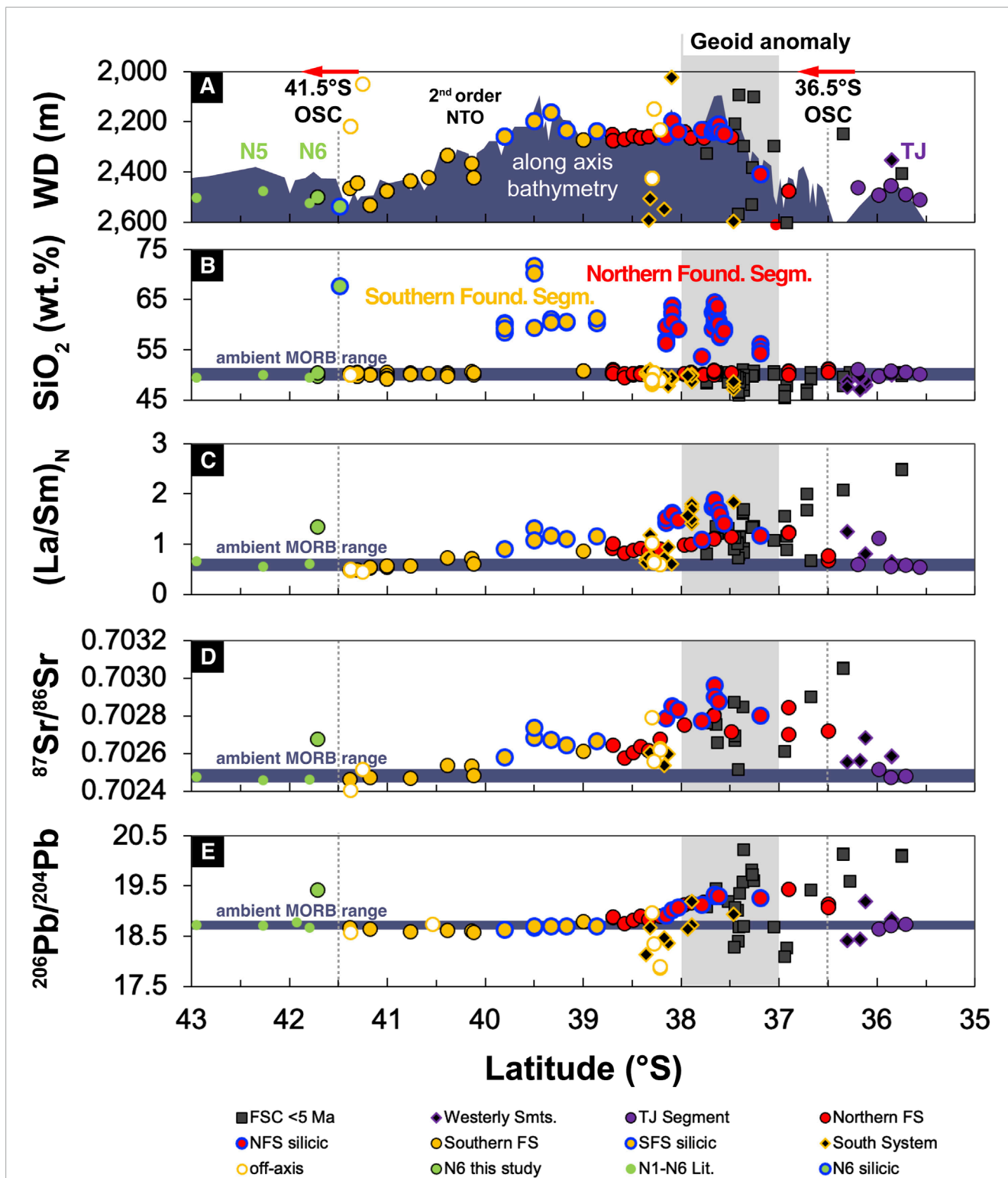
FIGURE 5
(A) Bathymetric profile (plotted versus degree latitude) of the PAR axis between the triple junction of the axis with the Juan Fernandez Microplate at 35.5°S and 43.0°S with sample locations. (B) SiO$_2$ (in wt.% and normalized to a total of 100 on a volatile-free basis), (C) Chondrite-normalized (La/Sm)$_N$ (normalizing values of Palme and O'Neill, 2003), (D) ^{87}Sr/^{86}Sr, and (E) ^{206}Pb/^{204}Pb along the PAR axis. Note the offset in SiO$_2$, incompatible trace elements (e.g., (La/Sm)$_N$) and ^{87}Sr/^{86}Sr isotopes between the silicic rocks (>52 wt.% SiO$_2$) and PAR tholeiites. Data of the southern PAR segments N5-N6 (south of the 41.5°S OSC) are from Klingelhoefer et al. (2006) and Hamelin et al. (2010). Also plotted in B-E are data of the near-ridge (<5 Ma; east of 115.0°W) intraplate lavas at their respective latitude. Note the oblique angle at which the FSC is approaching the ridge.

material into the axial melting zones enhances magma supply and thus promotes coupled assimilation-fractional crystallisation (AFC) processes (Freund et al., 2013). However, we observe subtle geochemical differences between the distinct occurrences of silicic rocks along the PAR axis.

The high SiO_2 contents are the result of enhanced magma differentiation and the fractionation of Fe-Ti oxides (Spulber and Rutherford, 1983; Juster et al., 1989; Hékinian et al., 1997; Berndt et al., 2005; Haase et al., 2005; Freund et al., 2013). However, Freund et al. (2013) identified differences in magma differentiation along the Foundation Segment that relate to the prevalence of simple fractional crystallization (SFX) versus combined assimilation and fractional crystallization (AFC) processes. Here, the enrichment in SiO_2 is controlled by the fractionation of Fe-Ti-rich oxides such as magnetite or ilmenite (Stoffers et al., 2002; Haase et al., 2005; Freund et al., 2013). Their onset of crystallization is controlled by $Fe^{3+}/\Sigma Fe$ and thus oxygen fugacity (e.g., Toplis and Carroll, 1995).

Spatially distinct suites of basalts record different evolutionary paths in Fe and Ti (the two elements most sensitive to the crystallization of oxide phases) with decreasing MgO along the Foundation Segment. Between 5.5 and 7.5 wt.% MgO, basalts from the northern portion of the segment record lower TiO_2 and FeO^t at given MgO and relative to the southern basalts and here especially those between 40.0 and 41.4°S (Figure 5). At MgO contents >7.5 wt.% the two groups converge, which excludes major differences in the Ti and Fe contents of their parental melts. A potential contribution of plume material can thus only be of minor importance as large additions of a Ti and Fe enriched HIMU-like plume source like Foundation (Devey et al., 1997) is expected to increase their relative abundance in the parental melts (cf. Jackson and Dasgupta, 2008). The divergence between the groups during magma differentiation can thus be interpreted as the result of subtle differences in oxygen fugacity: Slightly more reducing conditions prevail at the southern Foundation Segment resulting in a suppressed, or at least delayed crystallization of Fe-Ti-rich oxides. Titanium and Fe thus behave more incompatibly during magma differentiation. If this is the case, only small contributions from a HIMU source would be sufficient as it contains almost four times higher H_2O contents than the depleted mantle (Salters and Stracke, 2004; Cabral et al., 2014). In addition, primary intraplate lavas from Hawaii record oxygen fugacities that are on average 0.66 log units higher than MORB magmas (Brounce et al., 2017) supporting evidence for an oxidized OIB source. Even though at Foundation only few samples have been analyzed for their H_2O content, a small but significant difference is observed between the two groups of basalts (0.26 wt.% for the southern and 0.36 wt.% for the northern basalts and for MgO = 7-8 wt.%; each n = 5). A recent study by O'Neill et al. (2024) emphasizes that subtle differences in H_2O content are enhanced by replenished, mixed, tapped crystallization (RMTX) processes in a crustal magma chamber, which would then result in a significant impact on major element chemistry. We conclude that such scenario is highly feasibly for the Foundation Segment. Alternatively, the differences in Ti and Fe could also be explained by local changes in the crustal processes controlling magma composition SFX or AFC processes (Figure 5). According to Freund et al. (2013), the northern basalts are affected by extensive AFC processes, whereas the southern basalts are

more consistent with an evolution without significant assimilation (SFX or RMTX).

To further explore the role of the Foundation Plume in promoting the formation of silicic lavas, we use the distinct trace element and radiogenic isotope ratios to distinguish between crustal processes and the mantle source. The two northern sites with silicic lavas (SiO_2 >52 wt.%, MgO <4 wt.%) are located in the center or the southern edge of the geoid anomaly related to the Foundation Plume (Figure 5A). They are characterized by high incompatible trace element ratios including $(La/Sm)_N$ (Figure 5C) and $(Ce/Yb)_N$, and $^{87}Sr/^{86}Sr$ (Figure 5D) that are offset from their spatially associated basalts (cf. Freund et al., 2013). However, in $^{143}Nd/^{144}Nd$ and $^{206}Pb/^{204}Pb$ (Figure 5E), spatially associated silicic and basaltic lavas record similar values. Their lower $^{143}Nd/^{144}Nd$ (~0.51300), higher $^{206}Pb/^{204}Pb$ (>19.00) and negative Δ7/4 relative to the ambient MORB array can thus be interpreted as geochemical evidence for the involvement of enriched plume material in their petrogenesis. The southern occurrence of silicic lavas stretches from 38.8 to 40.0°S and is >100 km away from the area where the FSC (North System) intersects the PAR. Samples from this southern location record high incompatible trace element ratios and $^{87}Sr/^{86}Sr$ similar to the other occurrences of silicic lavas. However, their Nd and Pb isotopic composition with higher $^{143}Nd/^{144}Nd$ (~0.51310), lower $^{206}Pb/^{204}Pb$ (<18.80) and positive Δ7/4 is indistinguishable from ambient MORB (Figures 4, 5). This clearly demonstrates that many incompatible elements including the REE and their respective ratios as well as radiogenic Sr isotopes are affected by crustal processes.

To further elaborate on these issues, we use the Dy/Dy* vs. $(Dy/Yb)_N$ diagram after Davidson et al. (2012); Figure 6A and the λ_N REE shape coefficients of O'Neill (2016); Figure 6B to discern primary compositional heterogeneity from secondary crustal modifications. Silicic lavas erupted along the Foundation Segment plot on a vector in the Dy/Dy* vs. $(Dy/Yb)_N$ diagram that confirms the importance of amphibole and/or clinopyroxene during petrogenesis (Figure 6A). Basalts of the northern and southern Foundation Segment also plot in two geochemically distinct groups that differ in light REE content with the northern group being more enriched as expected for a plume influenced setting (Figure 6A). The older FSC lavas (>5 Ma or west of 115°W) record a trajectory towards a mantle source with residual garnet and are extending into the OIB field after Davidson et al. (2012); $(Dy/Yb)_N$ >1.6. The FSC lavas <5 Ma (plume-ridge interaction) are transitional between the Foundation Segment MORBs and the OIB field. This geochemical pattern can be reproduced by a simplistic mixing model using the composition of sample SO213 3VSRa from the TJ Segment as the depleted (MORB) and of sample SO100 58DS1 from Kelvin Seamount at 116.82°W as the enriched (OIB) endmember. In this case, the northern Foundation Segment basalts could be the product of adding 10%–30% of an OIB melt to the depleted MORB magma whereas the young FSC lavas record highly variable degrees of mixing ranging from purely depleted (MORB-like) to purely enriched (OIB). We note that the actual endmembers may be more extreme than our sample selection.

O'Neill (2016) uses polynomial fits to the full REE patterns instead of focusing on the ratios of individual middle to heavy REEs. Three of the resulting λ_N shape coefficients are sufficient to capture REE patterns at an accuracy of ±5%. These three terms are
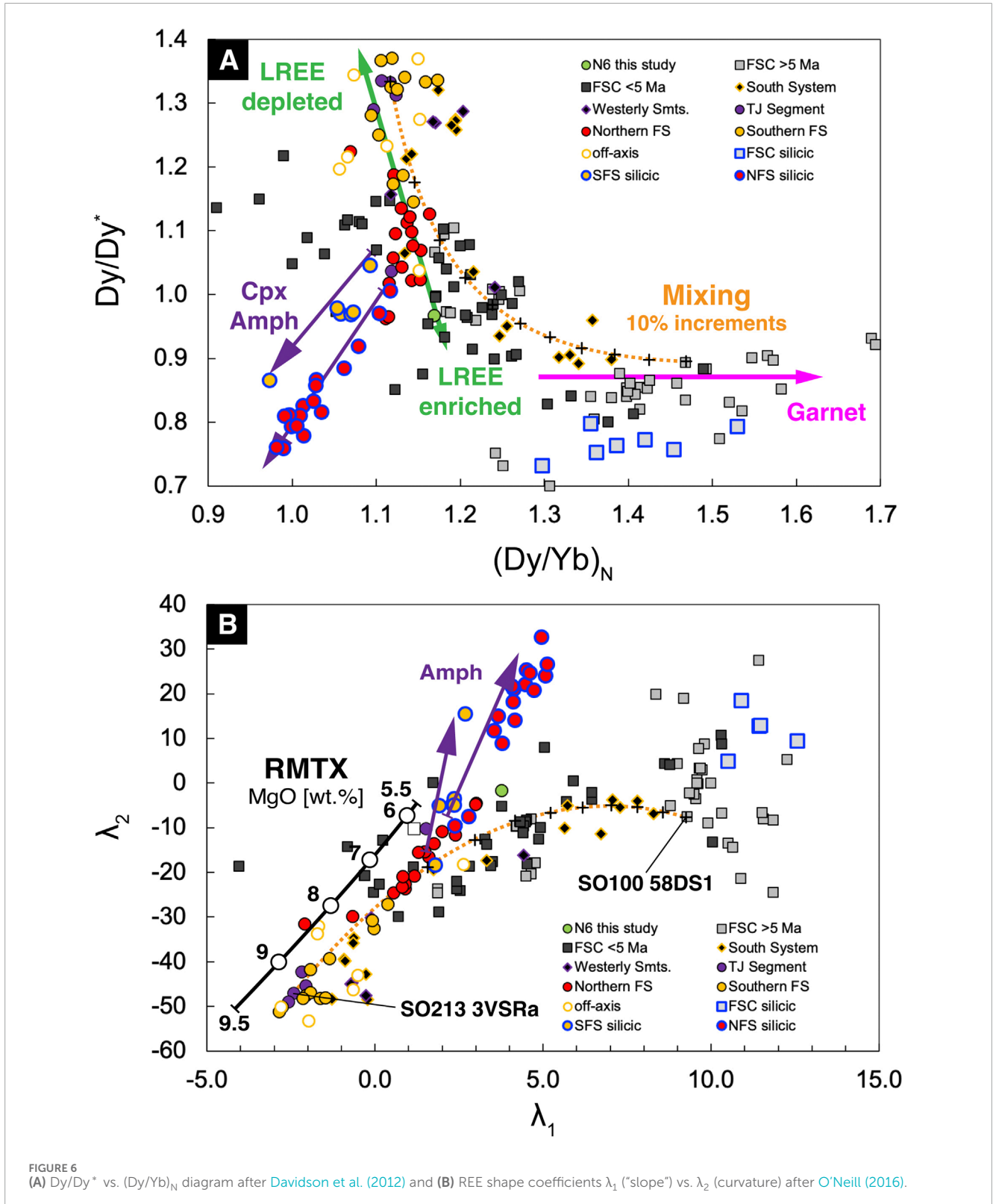
FIGURE 6
(A) Dy/Dy* vs. (Dy/Yb)$_N$ diagram after Davidson et al. (2012) and (B) REE shape coefficients λ_1 ("slope") vs. λ_2 (curvature) after O'Neill (2016).

λ_0, λ_1 and λ_2 and describe the abundance, slope and curvature of the respective REE pattern (O'Neill, 2016). Whereas λ_0 is intimately related to degree of differentiation (or MgO), diagrams of λ_1 vs. λ_2 are particularly useful to educate on petrogenetic processes and

source features. In Figure 6B, we show the FSC and Foundation Segment lavas in this context. In λ_1 vs. λ_2, the older FSC lavas are offset from the MORB array towards higher λ_1 (Figure 6B), which is consistent with other South Pacific OIBs and points towards a

garnet peridotite source (cf. O'Neill, 2016). Alternatively, to the scenario of mixing plume material into the axial melting zone to reproduce the geochemical differences between the north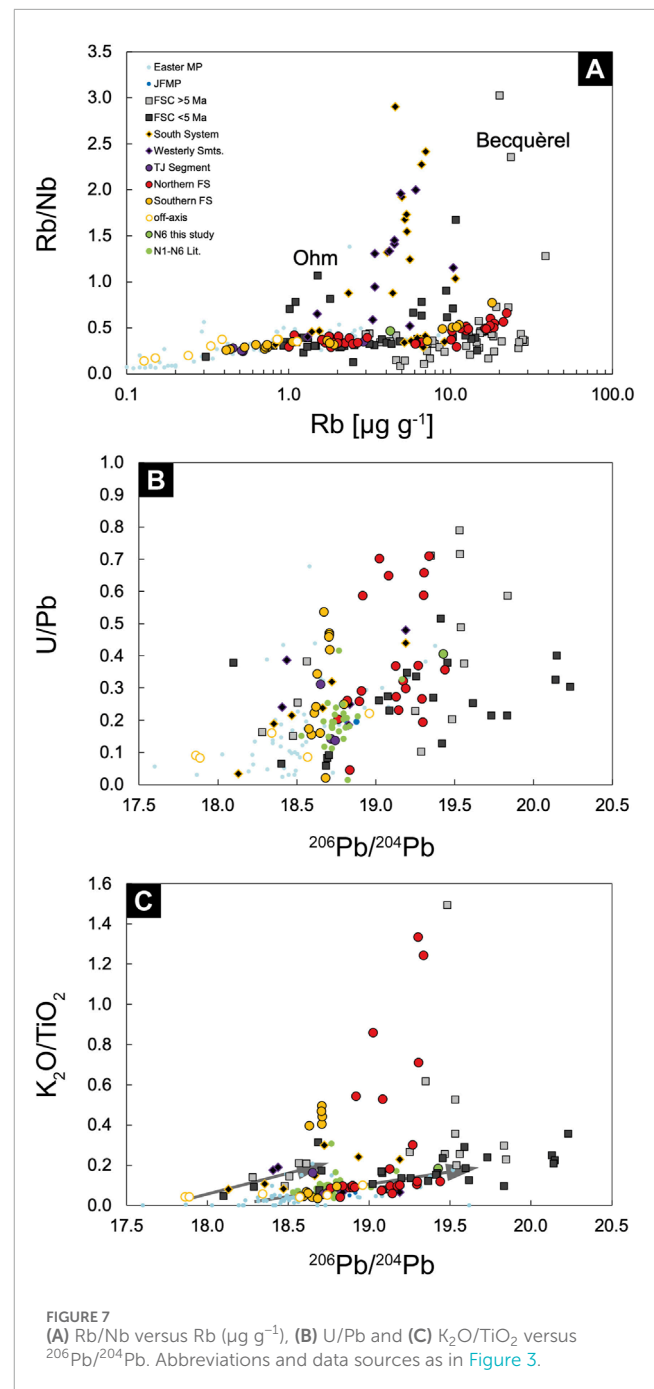ern and southern Foundation Segment basalts, the covariation in λ_1 vs. λ_2 could also result from RMTX processes in the magma system (Figure 6B). However, the lack of any systematic variation in MgO (and thus degree of differentiation) along the Foundation Segment or between the two distinct groups indicate that magma mixing is the more likely process. In contrast to Dy/Dy* vs. (Dy/Yb)$_N$, the λ_1 vs. λ_2 diagram helps to discriminate between the involvement of amphibole and clinopyroxene. Silicic lavas from the Foundation Segment plot on a trajectory that is consistent with the steep amphibole trajectory of O'Neill (2016 Figure 6B). This finding is in agreement with previous studies focusing on the formation of silicic lavas along the Foundation Segment (Haase et al., 2005; Freund et al., 2013). The small but significant offset between the northern and southern silicic lavas in Figures 6A, B points towards differences in the amount or type of plume material mixed into the axial melting zone.

4.3 Constraints on source composition

The enriched, plume-derived component is characterized by high $^{206}Pb/^{204}Pb$ at low $^{87}Sr/^{86}Sr$, negative Δ7/4 [deviation of the $^{207}Pb/^{204}Pb$ from the Northern Hemisphere Reference Line (NHRL) of Hart (1984)], high Ce/Pb and U/Pb but low Ba/Nb and Rb/Nb. These characteristics are consistent with a HIMU (high-μ = high $^{238}U/^{204}Pb$) mantle component (Devey et al., 1997) that is generally considered to have evolved from recycling of subduction-modified oceanic crust over long time scales (>>500 Ma; e.g., Thirlwall, 1997; Stracke et al., 2005). A HIMU component also fits with the proposed common origin of the Foundation Plume and the plume producing the southern Austral chain (>34; O'Connor et al., 1998), which is the type locality of HIMU (Stracke et al., 2005).

Whereas the most depleted FSC lavas ($^{206}Pb/^{204}Pb$ <18.50) plot below the NHRL in Pb-Pb isotope diagrams (negative Δ7/4 and Δ8/4), depleted off-axis samples show negative Δ8/4 but positive Δ7/4 similar to other depleted PAR and EPR samples far from the intersection with the FSC (Figure 3). However, there are significant differences in the composition of the depleted axial lavas and those erupted off-axis or intraplate. The latter group records lower SiO$_2$ contents than on-axis samples (Figure 2). Axial lavas from the southern Foundation, TJ and N1 to N6 segments of the PAR as well as the Juan Fernandez Microplate converge at a $^{206}Pb/^{204}Pb$ of 18.60–18.80, $^{87}Sr/^{86}Sr$ of 0.70244–0.70252 and $^{143}Nd/^{144}Nd$ of 0.51309–0.51312. Depleted intraplate and off-axis samples are characterized by low $^{206}Pb/^{204}Pb$ <18.50, but higher $^{87}Sr/^{86}Sr$ (0.70254–0.70263) and variable $^{143}Nd/^{144}Nd$ (0.51305–0.51314) relative to the depleted axial samples. Incompatible trace element ratios such as (La/Sm)$_N$ or Nb/Zr in these basalts are similar to those recorded in the depleted axial samples with the exception of Rb/Nb (higher; Figure 7A), U/Pb (lower; Figure 7B) and K$_2$O/TiO$_2$ (Figure 7C). Here, the axial basalts show a correlation in K$_2$O/TiO$_2$ versus $^{206}Pb/^{204}Pb$ extending from ratios of 0.04 and 18.57 to 0.12 and 19.44, respectively, whereas the off-axis/depleted intraplate lavas are offset to lower $^{206}Pb/^{204}Pb$ but higher K$_2$O/TiO$_2$ of 0.04 at a $^{206}Pb/^{204}Pb$ of ~17.90 and

FIGURE 7
(A) Rb/Nb versus Rb (μg g^{-1}), (B) U/Pb and (C) K$_2$O/TiO$_2$ versus $^{206}Pb/^{204}Pb$. Abbreviations and data sources as in Figure 3.

0.15 at ~18.50 (Figure 7C). Also, in the REE shape coefficients λ_1 and λ_2 we observe this offset between these two suites with the off-axis/depleted intraplate lavas plotting at higher λ_1 at a given λ_2.

Even though some of these geochemical indicators may be prone to crustal modifications (see above), the wide range in Sr-Pb and Nd-Pb isotope plots at low $^{206}Pb/^{204}Pb$ cannot be explained by simple binary mixing of two components. There are several lines of evidence suggesting that there is more than one low $^{206}Pb/^{204}Pb$ component involved in the Foundation-PAR system. Whereas most of the isotopic variability observed in FSC and PAR lavas is best explained by mixing an enriched (HIMU-like) OIB with a depleted MORB

mantle source, the low $^{206}Pb/^{204}Pb$ of off-axis and intraplate lavas are inconsistent with mixing between these two endmembers. The high Rb/Nb (Figure 7A) but low U/Pb and $^{206}Pb/^{204}Pb$ (Figure 7B) at elevated $^{87}Sr/^{86}Sr$ in conjunction with higher K_2O/TiO_2 and a mild light REE enrichment may point towards a mantle component with an EM1 flavour (cf. Stracke et al., 2005; Willbold and Stracke, 2006; Jackson and Dasgupta, 2008).
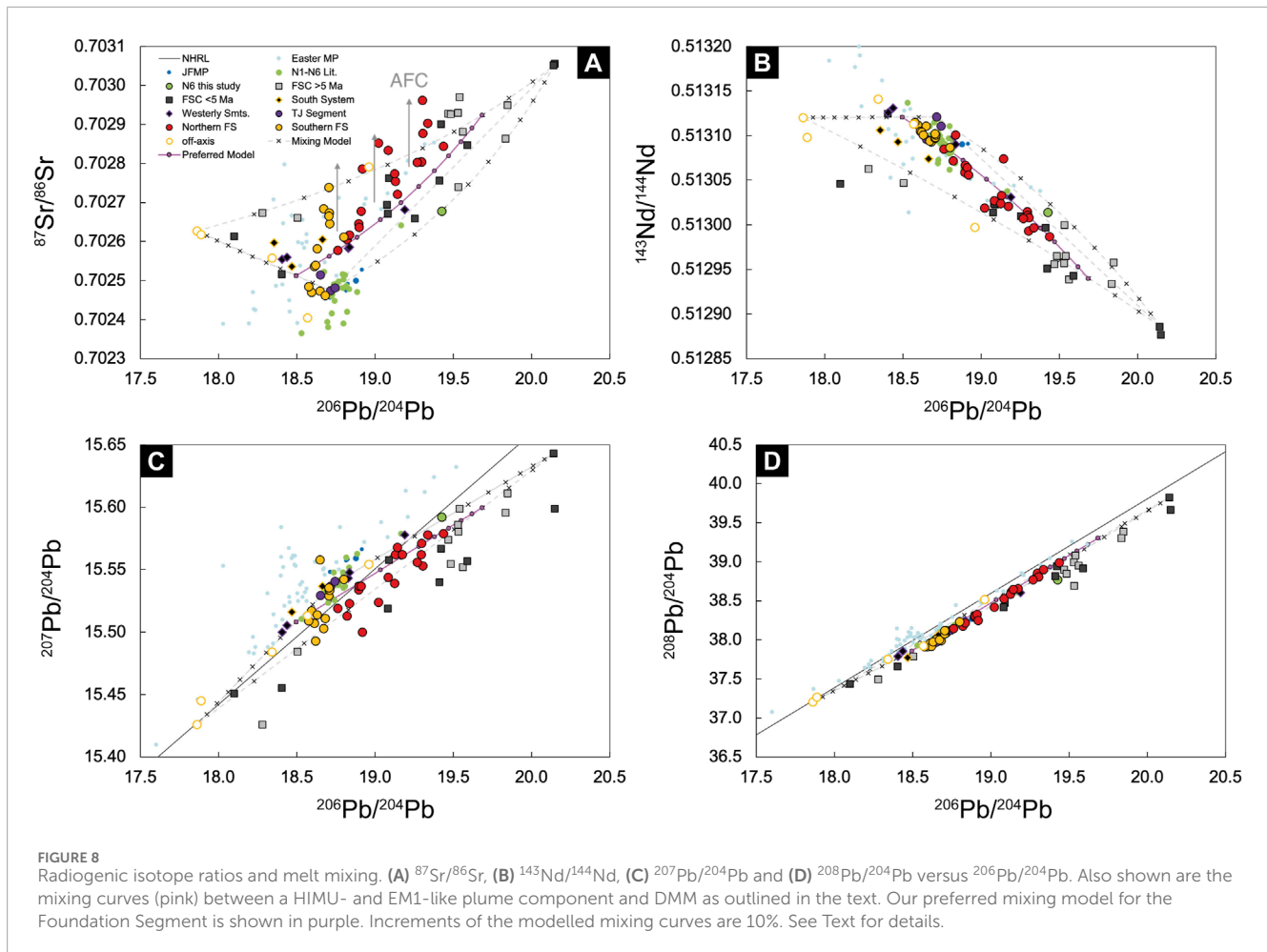
4.4 Tapping of the plume

A similar geodynamic setting to that of the Foundation-PAR plume ridge interaction may be found further north. Here, the ridge migration and the interaction between the East Pacific Rise (EPR; and to the same extent the PAR) and the so-called South Pacific Superswell – a region with a large geoid and lower mantle shear wave velocity anomaly, and numerous hotspots (e.g., McNutt and Judge, 1990) – may enhance the return flow to the spreading center along asthenospheric channels (e.g., Janney et al., 2000; Toomey et al., 2002; Harmon et al., 2011). Ridge-perpendicular convection and/or migrating melting anomalies along these channels (in addition to the possible extension of the upper plate) produces intraplate seamount chains such as the Pukapuka or Sojourn Ridges that are aligned parallel to the direction of absolute plate motion (Sandwell et al., 1995; Forsyth et al., 2006). These seamounts and the Rano Rahi seamount province west of the southern EPR as a whole are thus not directly related to a hotspot origin (Sandwell et al., 1995; Scheirer et al., 1996; Forsyth et al., 2006). However, the systematic changes in volcano morphology along these ridges are similar to those observed along the FSC. Seamounts located several hundred kilometers away from the ridge axis are generally conical and can rise up to 4,000 m above the surrounding seafloor. Towards the ridge, the volcanic morphology transitions towards more elongate and finally to volcanic ridges with summit heights of less than 1,500 m (cf. Sandwell et al., 1995; Devey et al., 1997; Hékinian et al., 1997). The Pukapuka Ridges and the FSC show both a linear radiometric age progression (O'Connor et al., 1998; Janney et al., 2000). Linear mixing between the mantle source underlying the eastern South Pacific Superswell ("Fozo"/"C") and EPR MORB is observed along the Pukapuka Ridges (Janney et al., 2000). The FSC, in contrast, records a combined HIMU-EM1 signature and geochemical mixing is evident only after the onset of plume-ridge interaction (O'Connor et al., 1998; Maia et al., 2005). Furthermore, westward migration of the PAR induces an asymmetric flow in the underlying viscous asthenosphere that extends mantle upwelling and enhances melt productivity on the advancing side of the axial melting region (e.g., Ito et al., 1997; Toomey et al., 2002; Carbotte et al., 2004). The PAR was thus able to tap the Foundation Plume over the last 5 Ma (at an initial distance of ~200 km). Since 1 Ma and possibly even since 2 Ma, plume material is diverted to the ridge axis (Maia et al., 2000; Maia and Arkani-Hamed, 2002). Currently, FSC intraplate lavas are restricted to the Pacific Plate with the exception of Rutherford Seamount that is part of the South System and as such may result from lithosphere flexuring (Maia et al., 2000) and related melting of an EM1 component at the edge of the plume.

4.5 Three-component mixing

The observation that the distinct enrichment of the mantle sources is combined with an increasing impact from crustal magmatic processes suggests that both the melting and melt ascent are significantly affected by plume-ridge interaction. The pooling of melts and the homogenization of individual magma batches during melt transport in channels – irrespective of their setting in a MOR axial melting zone or plume-ridge interaction – and in magma systems could result in falsified binary mixing arrays (Maclennan, 2008; Rudge et al., 2013). Studies of olivine-hosted melt inclusions from areas of plume-ridge interaction have demonstrated that the true range of heterogeneity – and here especially that of the more depleted compositions – remains obscured in bulk rock samples (Maclennan, 2008; Stracke et al., 2019). Because the apparent mixing endmembers may themselves be generated by mixing, binary mixing arrays (with the exception of isotope ratios of the same element such as Pb-Pb) may not reflect distinct compositional entities in the solid mantle (Rudge et al., 2013). Thus, the extremes of the melt compositions erupted along the Foundation Segment must be seen as minimum constraints of the chemical variability in the mantle source.

Here we propose that the compositions of the geochemically most extreme samples are themselves a product of pooled and mixed melt batches. However, we use the geochemical diversity to infer first-order mixing relationships between pooled melts dominated by the Foundation Plume sources and those dominated by ambient PAR mantle source (a.k.a. DMM). We use the composition of sample SO213 3VSRa (7.6 wt.% MgO) from the TJ Segment to the north of the Foundation Segment with $^{87}Sr/^{86}Sr$ = 0.70247, $^{143}Nd/^{144}Nd$ = 0.51312 and Pb isotope ratios ($^{206}Pb/^{204}Pb$, $^{207}Pb/^{204}Pb$ and $^{208}Pb/^{204}Pb$) of 18.72, 15.54 and 38.09 for DMM. The isotope composition of this sample is considered to be unaffected by plume-ridge interaction (Figure 5). The enriched endmember is represented by sample SO100-70DS1 (5.9 wt.% MgO) from Mendel Seamount with $^{87}Sr/^{86}Sr$ = 0.70305, $^{143}Nd/^{144}Nd$ = 0.51288 and Pb isotope ratios of 20.14, 15.64 and 39.83. We chose a sample from Mendel Seamount (at 113.93°W) over SO100 58DS1 (Kelvin Seamount at 116.82°W) used in the trace element modelling as the seamounts records the most enriched (high Sr and Pb, low Nd) isotope ratios. This sample is considered to reflect a melt derived from the HIMU-component of the Foundation plume. The EM1-flavoured component is tapped by the off-axis and depleted (with respect to Pb isotopes) intraplate lavas and we chose sample SO157 34DS1 collected between Planck Seamount (South System) and the PAR axis at 38.21°S. The high MgO content (9.65 wt.%) of this sample indicates a near primary melt origin and its isotopic composition is 0.70263 in $^{87}Sr/^{86}Sr$, 0.51312 in $^{143}Nd/^{144}Nd$ and Pb isotope ratios of 17.86, 15.43 and 37.21.

To model isotopic mixing between these two virtual endmembers, we used Sr, Nd, and Pb contents from the three distinct magmatic suites (FSC: HIMU, PAR: DMM, off-axis: EM1) extrapolated to 10 wt.% MgO and assuming incompatible (exponential) behavior (cf. O'Neill and Jenner, 2012). The resulting Sr, Nd, Pb contents for the virtual primitive melt are 200, 10 and 0.6 $\mu g\,g^{-1}$ for the HIMU, 150, 6 and 0.25 $\mu g\,g^{-1}$ for the DMM, and 200, 7 and 0.35 $\mu g\,g^{-1}$ for the EM1 component. The mixing

FIGURE 8
Radiogenic isotope ratios and melt mixing. **(A)** $^{87}Sr/^{86}Sr$, **(B)** $^{143}Nd/^{144}Nd$, **(C)** $^{207}Pb/^{204}Pb$ and **(D)** $^{208}Pb/^{204}Pb$ versus $^{206}Pb/^{204}Pb$. Also shown are the mixing curves (pink) between a HIMU- and EM1-like plume component and DMM as outlined in the text. Our preferred mixing model for the Foundation Segment is shown in purple. Increments of the modelled mixing curves are 10%. See Text for details.
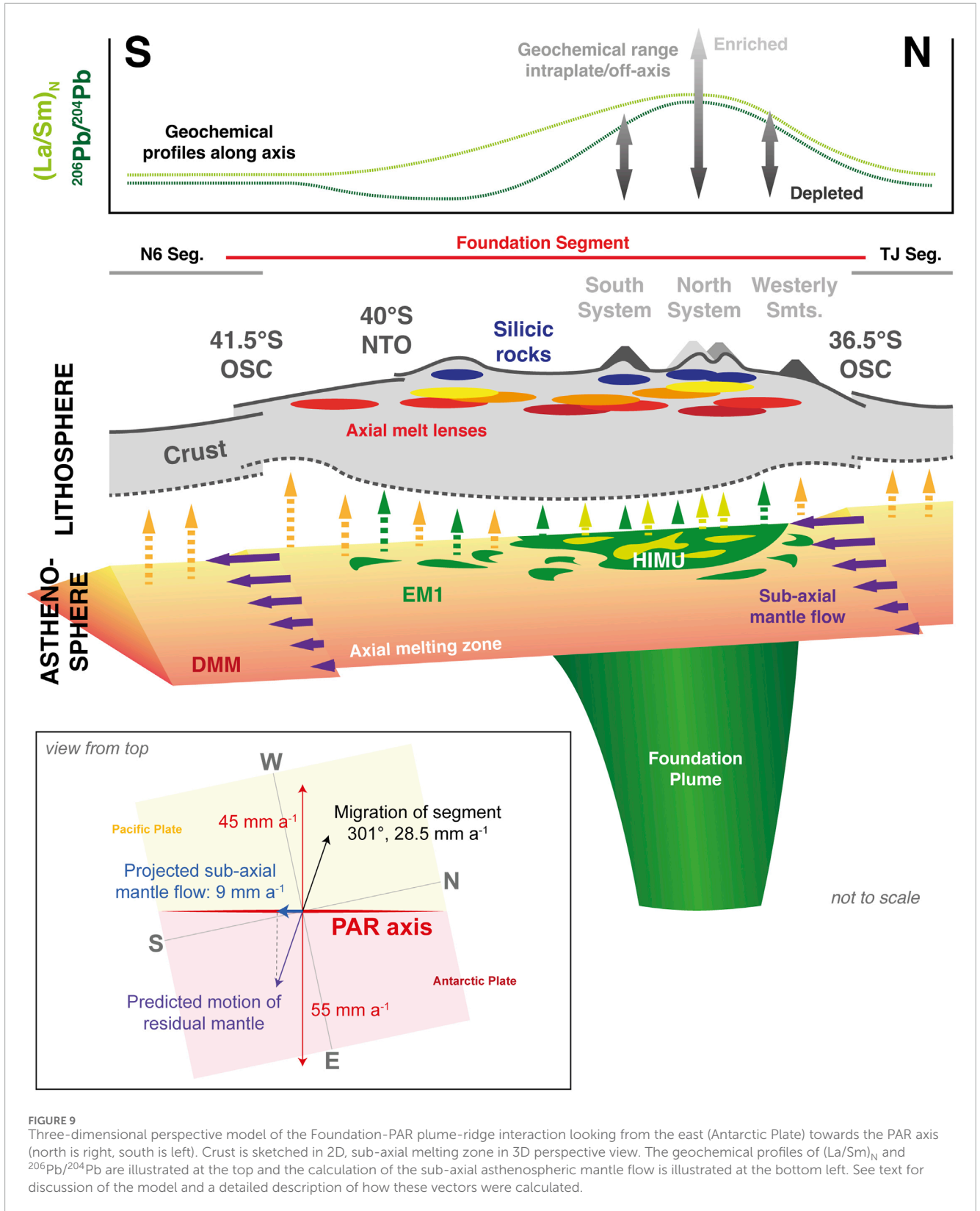
lines form a triangle that encloses almost all samples from the Foundation area (Figure 8). The mixing processes at the Foundation-PAR plume ridge interaction are (Figure 8): 1) Samples from the TJ Segment reflect the isotopic composition of the depleted (ambient) MORB mantle as its isotopic array overlaps with the depleted MORB samples from the Juan de Fuca Microplate to the north, as well as the N1-N6 Segments south of Foundation. 2) The lower $^{206}Pb/^{204}Pb$ and higher $^{87}Sr/^{86}Sr$ of basalts erupted at the southern Foundation Segment between 40 and 41°S are the result of mixing of up to 20% of melt derived from the EM1 plume component into the primitive MORB melt. 3) Northwards, the HIMU-derived melt component carries high $^{206}Pb/^{204}Pb$ at negative Δ7/4 and Δ8/4 and becomes increasingly mixed into the ridge axis. 4) The low $^{206}Pb/^{204}Pb$ and $^{143}Nd/^{144}Nd$ at elevated $^{87}Sr/^{86}Sr$ of intraplate lavas of the South System, the Westerly Seamounts, individual FSC edifices (e.g., Ohm, Becquèrel) as well as Foundation Segment off-axis lavas are consistent with an increasing proportion of an EM1-like plume component. 5) Silicic rocks of the PAR axis have elevated $^{87}Sr/^{86}Sr$ due to AFC processes and are thus not directly related to the mantle source. 6) Axial samples are dominated by melts derived from a DMM source and show a maximum plume melt contribution of 20%–30%; this plume contribution changes from HIMU-dominated in the center of plume-interaction to EM1-dominated towards the edges. 7) FSC lavas in contrast show a dominant proportion of plume-derived melts from variable proportions

of HIMU to EM1 but may also include variable amounts of a DMM-derived melt.

The presence of the EM1-component at the ridge axis where a lithospheric mantle is absent, further implies that it is part of the asthenospheric mantle (in this case plume material). This is in contrast to some other intraplate settings such as the Canary Islands where the EM1-component has been attributed to an upper lithospheric mantle origin (cf. Hoernle et al., 1991). Moreover, the presence of this EM1-component in intraplate lavas to the north (Westerly Seamounts) and south (South System and off-axis samples) of the center of plume-ridge interaction where the HIMU-component prevails can be interpreted to result from a concentric zoning of the Foundation plume.

4.6 Implications of the mixing model on the geochemical gradients

The geochemical signal of the plume is extending much further south than north indicating a highly asymmetric dispersal of plume material (irrespective of whether this relates to mixing of melts or solids) along the axis. We identified three distinct mantle components, two derived from melting of the Foundation plume and one from melting the ambient depleted mantle. The geochemical signal of the plume components is restricted to the Foundation

FIGURE 9
Three-dimensional perspective model of the Foundation-PAR plume-ridge interaction looking from the east (Antarctic Plate) towards the PAR axis (north is right, south is left). Crust is sketched in 2D, sub-axial melting zone in 3D perspective view. The geochemical profiles of $(La/Sm)_N$ and $^{206}Pb/^{204}Pb$ are illustrated at the top and the calculation of the sub-axial asthenospheric mantle flow is illustrated at the bottom left. See text for discussion of the model and a detailed description of how these vectors were calculated.

Segment which contrasts a mixing of melts across the overlapping limbs of an OSC (VanderBeek et al., 2016). However, plume dispersal along the Foundation Segment is highly asymmetric: to the north the incompatible trace element and radiogenic isotope signal of the plume are restricted to within 100 km from the center of plume-ridge interaction marked by the intersection of the North Ridge with the PAR axis (~37.5°S). To the south enriched (plume-derived) Pb isotope ratios, high U/Pb and low Rb/Nb are observed

up to 150 km, but other geochemical tracers (e.g., Nb/Zr, (La/Sm)$_N$, ^{87}Sr/^{86}Sr) of an OIB source extend farther than 300 km south. We interpret these different signals by a switch in the dominant plume source contributing to the erupted lavas. This switch affects some incompatible trace elements and radiogenic isotopes (e.g., U/Pb, Rb/Nb, Pb isotopes) but not others (e.g., Nb/Zr, (La/Sm)$_N$; Willbold and Stracke, 2006). At the center of the plume, the HIMU-component is dominant, whereas towards the edges of the plume, the EM1 component prevails. This model is consistent with recent models that attribute these isotopic endmembers to different source lithologies that show different behavior during mantle upwelling and melting. The HIMU component is considered to be derived from a silica-undersaturated garnet-peridotite or eclogite that originated from the recycling of pure igneous oceanic crust (e.g., Hofmann and White, 1982; Stracke et al., 2003; Jackson and Dasgupta, 2008). Melting experiments (e.g., Hirschmann et al., 2003; Kogiso et al., 2003) have demonstrated that this component has a lower solidus than peridotite and is likely to be the first phase to melt in an upwelling plume (e.g., Ito and Mahoney, 2005; Stracke and Bourdon, 2009; Jones et al., 2017). In addition, the excess density of recycled crust would result in its preferential sampling (from the lowermost mantle) in the inner plume conduit which is also the hottest portion of the plume (Jones et al., 2016). It is thus likely that a HIMU plume component would be concentrated in the center of a mantle plume and would contribute disproportionally to the melting (Figure 9). The EM component, in contrast is likely to be derived from the recycling of oceanic crust but including minor amounts of sediment of variable composition (Stracke et al., 2003 and references therein). Its solidus temperature is sensitive to composition but is considered to be higher than that of the HIMU source and lower or higher than that of the depleted upper mantle (e.g., Ito and Mahoney, 2005; Jones et al., 2017). Its contribution to melting relative to the depleted upper mantle is thus uncertain but melting is very likely in an axial melting zone where high degrees of partial melting are reached at shallower mantle depths.

In this framework, we can easily explain the differences between the distinct geochemical tracers along the Foundation Segment. At the center of plume ridge interaction, we find the strongest signal of the HIMU component. With increasing distance, we find a decrease in Pb isotopes and trace element ratios uniquely attributed to HIMU whereas other trace element and isotope ratios that are common to all OIB sources (cf. Willbold and Stracke, 2006) remain elevated above the background level of ambient MORB (Figure 5). Lower U/Pb and ^{206}Pb/^{204}Pb but higher Rb/Nb and ^{87}Sr/^{86}Sr are consistent with a change in the dominant plume component from HIMU to EM1. The general decrease with distance is then a function of the plume becoming progressively diluted by melt depletion along the axis (cf. Shorttle et al., 2010; Figure 9) before the plume signal disappears at the two OSCs bounding the Foundation Segment.

4.7 Effects of ridge migration on plume dispersal

One crucial unique feature of the Foundation-PAR plume-ridge interaction is the asymmetric dispersal of the plume with a preferential flow directed to the south along the Foundation

Segment (Maia et al., 2000; this study). In intraplate settings, an asymmetry of plume dispersal is commonly attributed to the effects of drag from the overlying, moving lithosphere (e.g., Sleep, 1996), which – in case of Foundation – would result in a westerly orientation parallel to the motion of the Pacific Plate. At mid-ocean ridges, however, the oblique migration of a ridge relative to the hotspot reference frame induces an additional along-axis component of asthenospheric mantle flow. This basic concept was first introduced by Schouten et al. (1987) and later adopted by Carbotte et al. (2008) to explain their observations along the intermediate-spreading Juan de Fuca Ridge where it interacts with the Cobb hotspot. Carbotte et al. (2008) argue that an induced sub-axial asthenospheric flow deviates plume material into a preferred (in this case southerly) direction thus altering the symmetric pattern expected for plumes interacting with intermediate-spreading mid-ocean ridges (cf. Ito et al., 2003). We use the model of Carbotte et al. (2008) to match the setting of the Foundation-PAR plume-ridge interaction. Currently, the Foundation Segment migrates at a rate of ~28.5 mm a^{-1} towards 301° (azimuth and velocity extracted from the plate motion reference frame of Müller et al. (2022); Figure 9). From a ridge-centered perspective the residual mantle would thus move into the opposite direction (121°). Projecting this vector onto the ridge axis would thus result in a southerly directed mantle flow on the order of ~9 mm a^{-1} (Figure 9). Even though the rate of the sub-axial asthenospheric flow is insufficient to explain the extent of the geochemical plume signal along the Foundation Segment, its orientation is in line with the observed asymmetry. The slower migration rate of the 36.5°S OSC relative to the 41.5°S OSC (cf. Maia et al., 2000) is the result of the competing forces of southward directed sub-axial flow (driving OSC migration) versus the push related to inflation and lengthening of the Foundation Segment in response to the inflow of plume material. However detailed studies of the crustal architecture and plume-ridge interaction over time are required to fully understand the geodynamic processes controlling plume dispersal at fast-spreading ridges.

5 Concluding remarks

The Foundation area at the northern termination of the PAR represents a rare example of a mantle plume being approached by and actively interacting with a fast-spreading mid-ocean ridge. Research cruise SO213 filled important gaps in the spatial sample coverage and the newly integrated dataset (Supplementary Table S1) allows for the first time to decipher the current state of the Foundation-PAR plume-ridge interaction. The Foundation Plume contributes compositionally distinct material that can be used as an inert tracer for geochemical mapping and modelling. The plume appears to be concentrically zoned with the HIMU-component confined to the center of the plume and a marginally prevailing EM1-component. Ubiquitous is the addition of melts derived from the ambient depleted upper mantle that results in a complex system where three component mix at variable proportions. The result is a partial decoupling of incompatible element ratios from and radiogenic isotopes (e.g., (La/Sm)$_N$ vs. ^{206}Pb/^{204}Pb) and of distinct isotope systems (e.g., Sr vs. Pb isotopes). We have demonstrated that the whole Foundation Segment of the PAR is influenced by

the plume and that the prevailing components (DMM-HIMU vs. DMM-EM1) are a function of distance from the center of plume-ridge interaction. The preferential deviation of plume material to the south is a result of ridge migration and the induced sub-axial flow. The influx of plume material into the ridge axis may further explain excess magmatism as expressed by the unusual length (~550 km) of the segment, crustal thickening and shallowing of the ridge axis, and intense hydrothermal activity at the center of plume-ridge interaction. The tectonic response to the increasing influx of plume material into the ridge may trigger rift propagation (non-transform offsets within the first-order segment). This preferential setting for crustal assimilation in combination with replenished, mixed, tapped crystallization (RMTX) processes in the axial magma chamber leads to the extensive occurrence of silicic rocks along this stretch of the PAR.

Data availability statement

The original contributions presented in the study are included in the Supplementary Material, further inquiries can be directed to the corresponding author.

Author contributions

PB: Conceptualization, Data curation, Investigation, Visualization, Writing–original draft, Writing–review and editing. CB: Conceptualization, Investigation, Supervision, Validation, Writing–review and editing. KH: Conceptualization, Data curation, Funding acquisition, Project administration, Resources, Supervision, Writing–review and editing. FG: Conceptualization, Validation, Writing–review and editing. FH: Methodology, Validation, Writing–review and editing. MR: Methodology, Validation, Writing–review and editing. CD: Data curation, Resources, Writing–review and editing. LR: Formal Analysis, Investigation, Software, Writing–review and editing.

Funding

Acknowledgments

Conflict of interest

The authors declare that the research was conducted in the absence of any commercial or financial relationships that could be construed as a potential conflict of interest.

Publisher's note

All claims expressed in this article are solely those of the authors and do not necessarily represent those of their affiliated organizations, or those of the publisher, the editors and the reviewers. Any product that may be evaluated in this article, or claim that may be made by its manufacturer, is not guaranteed or endorsed by the publisher.

Supplementary material

The Supplementary Material for this article can be found online at: https://www.frontiersin.org/articles/10.3389/feart.2024.1456429/full#supplementary-material

References

Beier, C., Vanderkluysen, L., Regelous, M., Mahoney, J. J., and Garbe-Schönberg, D. (2011). Lithospheric control on geochemical composition along the Louisville Seamount Chain. *Geochem. Geophys. Geosystems* 12, Q0AM01. doi:10.1029/2011GC003690

Berndt, J., Koepke, J., and Holtz, F. (2005). An experimental investigation of the influence of water and oxygen fugacity on differentiation of MORB at 200 MPa. *J. Petrology* 46, 135–167. doi:10.1093/petrology/egh066

Brandl, P. A., Regelous, M., Beier, C., and Haase, K. M. (2013). High mantle temperatures following rifting caused by continental insulation. *Nat. Geosci.* 6, 391–394. doi:10.1038/ngeo1758

Briais, A., and Rabinowicz, M. (2002). Temporal variations of the segmentation of slow to intermediate spreading mid-ocean ridges 1. Synoptic observations based on satellite altimetry data. *J. Geophys. Res.* 107, 431–519. doi:10.1029/2001JB000533

Brounce, M., Stolper, E., and Eiler, J. (2017). Redox variations in Mauna Kea lavas, the oxygen fugacity of the Hawaiian plume, and the role of volcanic gases in Earth's oxygenation. *Proc. Natl. Acad. Sci.* 114, 8997–9002. doi:10.1073/pnas.1619527114

Cabral, R. A., Jackson, M. G., Koga, K. T., Rose-Koga, E. F., Hauri, E. H., Whitehouse, M. J., et al. (2014). Volatile cycling of 2, CO_2, F, and Cl in the HIMU mantle: a new window provided by melt inclusions from oceanic hot spot lavas at Mangaia, Cook Islands. *Geochem. Geophys. Geosystems* 15, 4445–4467. doi:10.1002/2014GC005473

Carbotte, S. M., Nedimović, M. R., Canales, J. P., Kent, G. M., Harding, A. J., and Marjanovic, M. (2008). Variable crustal structure along the Juan de Fuca Ridge: Influence of on-axis hot spots and absolute plate motions. *Geochem. Geophys. Geosystems* 9, Q08001. doi:10.1029/2007GC001922

Carbotte, S. M., Small, C., and Donnelly, K. (2004). The influence of ridge migration on the magmatic segmentation of mid-ocean ridges. *Nature* 429, 743–746. doi:10.1038/nature02652

Courtillot, V., Davaille, A., Besse, J., and Stock, J. (2003). Three distinct types of hotspots in the Earth's mantle. *Earth Planet. Sci. Lett.* 205, 295–308. doi:10.1016/S0012-821X(02)01048-8

Cushman, B., Sinton, J., Ito, G., and Dixon, J. E. (2006). Glass compositions, plume-ridge interaction, and hydrous melting along the Galápagos Spreading Center, 90.5°W to 98°W. *Geochem. Geophys. Geosyst.* 5. doi:10.1029/2004GC000709

Davidson, J., Turner, S., and Plank, T. (2012). Dy/Dy∗: variations arising from mantle sources and petrogenetic processes. *J. Petrology* 54, 525–537. doi:10.1093/petrology/egs076

Devey, C. W., Hékinian, R., Ackermand, D., Binard, N., Francke, B., Hémond, C., et al. (1997). The Foundation Seamount chain: a first survey and sampling. *Mar. Geol.* 137, 191–200. doi:10.1016/S0025-3227(96)00104-1

Forsyth, D. W., Harmon, N., Scheirer, D. S., and Duncan, R. A. (2006). Distribution of recent volcanism and the morphology of seamounts and ridges in the GLIMPSE study area: implications for the lithospheric cracking hypothesis for the origin of intraplate, non–hot spot volcanic chains. *J. Geophys. Res. Solid Earth* 111, 1978–2012. doi:10.1029/2005JB004075

Fretzdorff, S., Worthington, T. J., Haase, K. M., Hékinian, R., Franz, L., Keller, R., et al. (2004). Magmatism in the bransfield basin: rifting of the South shetland arc? *J. Geophys. Res.* 109, B12208. doi:10.1029/2004JB003046

Freund, S., Beier, C., Krumm, S., and Haase, K. M. (2013). Oxygen isotope evidence for the formation of andesitic–dacitic magmas from the fast-spreading Pacific–Antarctic Rise by assimilation–fractional crystallisation. *Chem. Geol.* 347, 271–283. doi:10.1016/j.chemgeo.2013.04.013

Garbe-Schönberg, C.-D. (1993). Simultaneous determination of thirty-seven trace elements in twenty-eight international rock standards by ICP-MS. *Geostand. Newsl.* 17, 81–97. doi:10.1111/j.1751-908x.1993.tb00122.x

Goldstein, S., O'nions, R., and Hamilton, P. (1984). A Sm-Nd isotopic study of atmospheric dusts and particulates from major river systems. *Earth Planet. Sci. ldots* 70, 221–236. doi:10.1016/0012-821x(84)90007-4Available at: http://linkinghub.elsevier.com/retrieve/pii/0012821X84900074.

Haase, K., Stoffers, P., and Garbe-Schonberg, C. (1997). The petrogenetic evolution of lavas from Easter Island and neighbouring seamounts, near-ridge hotspot volcanoes in the SE Pacific. *Journal of Petrology* 38, 785–813. doi:10.1093/petroj/38.6.785

Haase, K. M., Brandl, P. A., Devey, C. W., Hauff, F., Melchert, B., Garbe-Schönberg, D., et al. (2016). Compositional variation and ^{226}Ra-^{230}Th model ages of axial lavas from the southern Mid-Atlantic Ridge, 8°48′S. *Geochemistry Geophysics Geosystems* 17, 199–218. doi:10.1002/2015GC006016

Haase, K. M., Stroncik, N. A., Hékinian, R., and Stoffers, P. (2005). Nb-depleted andesites from the Pacific-Antarctic Rise as analogs for early continental crust. *Geology* 33, 921–924. doi:10.1130/G21899.1

Hamelin, C., Dosso, L., Hanan, B., Barrat, J.-A., and Ondréas, H. (2010). Sr-Nd-Hf isotopes along the pacific Antarctic Ridge from 41 to 53°S. *Geophysical Research Letters* 37, L10303. doi:10.1029/2010GL042979

Hanan, B. B., and Schilling, J. (1989). Easter microplate evolution: Pb isotope evidence. *J. Geophys. Res.* 94, 7432–7448. doi:10.1029/JB094iB06p07432

Harmon, N., Forsyth, D. W., Weeraratne, D. S., Yang, Y., and Webb, S. C. (2011). Mantle heterogeneity and off axis volcanism on young Pacific lithosphere. *Earth and Planetary Science Letters* 311, 306–315. doi:10.1016/j.epsl.2011.09.038

Hart, S. R. (1984). A large-scale isotope anomaly in the Southern Hemisphere mantle. *Nature* 309, 753–757. doi:10.1038/309753a0

Hékinian, R., Stoffers, P., Ackermand, D., Révillon, S., Maia, M., and Bohn, M. (1999). Ridge–hotspot interaction: the Pacific–Antarctic Ridge and the foundation seamounts. *Marine Geology* 160, 199–223. doi:10.1016/S0025-3227(99)00027-4

Hékinian, R., Stoffers, P., Devey, C., Ackermand, D., Hemond, C., O'Connor, J., et al. (1997). Intraplate versus ridge volcanism on the pacific-Antarctic Ridge near 37°S–111°W. *Journal of Geophysical Research* 102, 12265–12286. doi:10.1029/96jb03856

Hirschmann, M., Kogiso, T., Baker, M., and Stolper, E. (2003). Alkalic magmas generated by partial melting of garnet pyroxenite. *Geology* 31, 481. doi:10.1130/0091-7613(2003)031<0481:amgbpm>2.0.co;2

Hoernle, K., Hauff, F., Kokfelt, T. F., Haase, K., Garbe-Schönberg, D., and Werner, R. (2011). On- and off-axis chemical heterogeneities along the South Atlantic Mid-Ocean-Ridge (5–11°S): shallow or deep recycling of ocean crust and/or intraplate volcanism? *Earth and Planetary Science Letters* 306, 86–97. doi:10.1016/j.epsl.2011.03.032

Hoernle, K., Tilton, G., and Schmincke, H.-U. (1991). SrNdPb isotopic evolution of Gran Canaria: evidence for shallow enriched mantle beneath the Canary Islands. *Earth and Planetary Science Letters* 106, 44–63. doi:10.1016/0012-821X(91)90062-M

Hofmann, A., and White, W. (1982). Mantle plumes from ancient oceanic crust. *Earth and Planetary Science Letters* 57, 421–436. doi:10.1016/0012-821x(82)90161-3

Ito, G., Lin, J., and Gable, C. W. (1996). Dynamics of mantle flow and melting at a ridge-centered hotspot: Iceland and the Mid-Atlantic Ridge. *Earth and Planetary Science Letters* 144, 53–74. doi:10.1016/0012-821X(96)00151-3

Ito, G., Lin, J., and Gable, C. W. (1997). Interaction of mantle plumes and migrating mid-ocean ridges: implications for the Galápagos plume-ridge system. *J. Geophys. Res.* 102, 15403–15417. doi:10.1029/97JB01049

Ito, G., Lin, J., and Graham, D. (2003). Observational and theoretical studies of the dynamics of mantle plume–mid-ocean ridge interaction. *Reviews of Geophysics* 41, 207. doi:10.1029/2002RG000117

Ito, G., and Mahoney, J. (2005). Flow and melting of a heterogeneous mantle: 1. Method and importance to the geochemistry of ocean island and mid-ocean ridge basalts. *Earth and Planetary Science Letters* 230, 29–46. doi:10.1016/j.epsl.2004.10.035

Jackson, M. G., and Dasgupta, R. (2008). Compositions of HIMU, EM1, and EM2 from global trends between radiogenic isotopes and major elements in ocean island basalts. *Earth and Planetary Science Letters* 276, 175–186. doi:10.1016/j.epsl.2008.09.023

Janney, P. E., Macdougall, J. D., Natland, J. H., and Lynch, M. A. (2000). Geochemical evidence from the Pukapuka volcanic ridge system for a shallow enriched mantle domain beneath the South Pacific Superswell. *Chemical Geology* 181, 47–60. doi:10.1016/S0012-821X(00)00181-3

Jones, T. D., Davies, D. R., Campbell, I. H., Iaffaldano, G., Yaxley, G., Kramer, S. C., et al. (2017). The concurrent emergence and causes of double volcanic hotspot tracks on the Pacific plate. *Nature Publishing Group* 545, 472–476. doi:10.1038/nature22054

Jones, T. D., Davies, D. R., Campbell, I. H., Wilson, C. R., and Kramer, S. C. (2016). Do mantle plumes preserve the heterogeneous structure of their deep-mantle source? *Earth and Planetary Science Letters* 434, 10–17. doi:10.1016/j.epsl.2015.11.016

Juster, T. C., Grove, T. L., and Perfit, M. R. (1989). Experimental constraints on the generation of FeTi basalts, andesites, and rhyodacites at the Galapagos Spreading Center, 85°W and 95°W. *Journal of Geophysical Research* 94, 9251–9274. doi:10.1029/jb094ib07p09251

Kelley, K. A., Kingsley, R., and Schilling, J.-G. (2013). Composition of plume-influenced mid-ocean ridge lavas and glasses from the mid-atlantic ridge, East Pacific rise, Galápagos spreading center, and gulf of aden. *Geochemistry Geophysics Geosystems* 14, 223–242. Available at:. doi:10.1002/ggge.20049

Kendrick, M. A., Hémond, C., Kamenetsky, V. S., Danyushevsky, L., Devey, C. W., Rodemann, T., et al. (2017). Seawater cycled throughout Earth's mantle in partially serpentinized lithosphere. *Nature Geoscience* 10, 222–228. doi:10.1038/ngeo2902

Kincaid, C., Schilling, J.-G., and Gable, C. (1996). The dynamics of off-axis plume-ridge interaction in the uppermost mantle. *Earth and Planetary Science Letters* 137, 29–43. doi:10.1016/0012-821X(95)00201-M

Kingsley, R. H., Blichert-Toft, J., Fontignie, D., and Schilling, J. (2007). Hafnium, neodymium, and strontium isotope and parent-daughter element systematics in basalts from the plume-ridge interaction system of the Salas y Gomez Seamount Chain and Easter Microplate. *Geochem Geophys Geosyst* 8, 2006GC001401. doi:10.1029/2006GC001401

Klein, E. M., and Langmuir, C. H. (1987). Global correlations of ocean ridge basalt chemistry with axial depth and crustal thickness. *Journal of Geophysical Research* 92, 8089–8115. doi:10.1029/jb092ib08p08089

Klingelhoefer, F., Ondréas, H., Briais, A., Hamelin, C., and Dosso, L. (2006). New structural and geochemical observations from the pacific-Antarctic Ridge between 52°45′S and 41°15′S. *Geophysical Research Letters* 33, L21312. doi:10.1029/2006GL027335

Kogiso, T., Hirschmann, M., and Frost, D. (2003). High-pressure partial melting of garnet pyroxenite: possible mafic lithologies in the source of ocean island basalts. *Earth and Planetary Science Letters* 216, 603–617. doi:10.1016/s0012-821x(03)00538-7

Kokfelt, T. F., Hoernle, K., Hauff, F., Fiebig, J., Werner, R., and Garbe-Schönberg, D. (2006). Combined trace element and Pb-Nd–Sr-O isotope evidence for recycled oceanic crust (upper and lower) in the Iceland mantle plume. *Journal of Petrology* 47, 1705–1749. doi:10.1093/petrology/egl025

Koppers, A. A. P., Becker, T. W., Jackson, M. G., Konrad, K., Müller, R. D., Romanowicz, B., et al. (2021). Mantle plumes and their role in Earth processes. *Nat Rev Earth Environ* 2, 382–401. doi:10.1038/s43017-021-00168-6

Labidi, J., Cartigny, P., Hamelin, C., Moreira, M., and Dosso, L. (2014). Sulfur isotope budget (32S, 33S, 34S and 36S) in Pacific-Antarctic ridge basalts: a record of mantle source heterogeneity and hydrothermal sulfide assimilation. *Geochimica et Cosmochimica Acta* 133, 47–67. doi:10.1016/j.gca.2014.02.023

Le Maitre, R. W., Streckeisen, A., Zanettin, B., and Le Bas, M. J. (2002). *Igneous rocks: a classification and glossary of terms*, 1–253.

Lonsdale, P. (1994). Geomorphology and structural segmentation of the crest of the southern (Pacific-Antarctic) East Pacific rise. *Journal of Geophysical Research* 99, 4683–4702. doi:10.1029/93JB02756

Macdougall, J. D., and Lugmair, G. W. (1985). Extreme isotopic homogeneity among basalts from the southern East Pacific Rise: mantle or mixing effect? *Nature* 313, 209–211. doi:10.1038/313209a0

Maclennan, J. (2008). Concurrent mixing and cooling of melts under Iceland. *Journal of Petrology* 49, 1931–1953. doi:10.1093/petrology/egn052Available at: http://petrology.oxfordjournals.org/cgi/content/abstract/egn052v1.

Maia, M., Ackermand, D., Dehghani, G. A., Gente, P., Hékinian, R., Naar, D., et al. (2000). The Pacific-Antarctic Ridge–Foundation hotspot interaction: a case study of a ridge approaching a hotspot. *Marine Geology* 167, 61–84. doi:10.1016/S0025-3227(00)00023-2

Maia, M., and Arkani-Hamed, J. (2002). The support mechanism of the young Foundation Seamounts inferred from bathymetry and gravity. *Geophysical Journal International* 149, 190–210. doi:10.1046/j.1365-246X.2002.01635.x

Maia, M., Dyment, J., and Jouannetaud, D. (2005). Constraints on age and construction process of the Foundation chain submarine volcanoes from magnetic modeling. *Earth and Planetary Science Letters* 235, 183–199. doi:10.1016/j.epsl.2005.02.044

Maia, M., Hemond, C., and Gente, P. (2001). Contrasted interactions between plume, upper mantle, and lithosphere: foundation chain case. *Geochemistry Geophysics Geosystems* 2. doi:10.1029/2000GC000117

McNutt, M. K., and Judge, A. V. (1990). The Superswell and mantle dynamics beneath the South Pacific. *Science* 248, 969–975. doi:10.1126/science.248.4958.969

Michael, P., and Chase, R. (1987). The influence of primary magma composition, H 2 O and pressure on mid-ocean ridge basalt differentiation. *Contributions to Mineralogy and Petrology* 96, 245–263. doi:10.1007/bf00375237

Mittelstaedt, E., and Ito, G. (2005). Plume-ridge interaction, lithospheric stresses, and the origin of near-ridge volcanic lineaments. *Geochemistry Geophysics Geosystems* 6, 4199. doi:10.1029/2004GC000860

Morgan, W. J. (1978). Rodriguez, Darwin, Amsterdam,, A second type of hotspot island. *Journal of Geophysical Research Solid Earth (1978–2012)* 83, 5355–5360. doi:10.1029/JB083iB11p05355

Müller, R. D., Flament, N., Cannon, J., Tetley, M. G., Williams, S. E., Cao, X., et al. (2022). A tectonic-rules-based mantle reference frame since 1 billion years ago – implications for supercontinent cycles and plate–mantle system evolution. *Solid Earth* 13, 1127–1159. doi:10.5194/se-13-1127-2022

Niu, Y., Wilson, M., Humphreys, E. R., and O'Hara, M. J. (2011). The origin of intra-plate Ocean Island basalts (OIB): the lid effect and its geodynamic implications. *Journal of Petrology* 52, 1443–1468. doi:10.1093/petrology/egr030

O'Connor, J. M., Stoffers, P., and Wijbrans, J. R. (1998). Migration rate of volcanism along the foundation chain, SE pacific. *Earth and Planetary Science Letters* 164, 41–59. doi:10.1016/S0012-821X(98)00165-4

O'Connor, J. M., Stoffers, P., and Wijbrans, J. R. (2001). Erratum to: "En echelon volcanic elongate ridges connecting intraplate Foundation Chain volcanism to the Pacific–Antarctic spreading center.". *Earth and Planetary Science Letters* 189, 633–648. doi:10.1016/S0012-821X(01)00348-X

O'Neill, H. S. C. (2016). The smoothness and shapes of chondrite-normalized rare earth element patterns in basalts. *Journal of Petrology* 57, 1463–1508. doi:10.1093/petrology/egw047

O'Neill, H.St. C., Berry, A. J., Danyushevsky, L. V., Falloon, T. J., Maas, R., and Feig, S. T. (2024). The relationship between iron redox states and H2O contents in back-arc basin basaltic glasses from the North Fiji Basin. *Chemical Geology* 655, 122062. doi:10.1016/j.chemgeo.2024.122062

O'Neill, H. S. C., and Jenner, F. E. (2012). The global pattern of trace-element distributions in ocean floor basalts. *Nature* 491, 698–704. doi:10.1038/nature11678

Palme, H., and O'Neill, H. S. C. (2003). "Cosmochemical estimates of mantle composition," in *Treatise on geochemistry*. Editors H. D. Holland, and K. K. Turekian (Amsterdam: Elsevier), 1–38. doi:10.1016/B0-08-043751-6/02177-0

Pollock, M. A., Klein, E. M., Karson, J. A., and Coleman, D. S. (2009). Compositions of dikes and lavas from the Pito Deep Rift: implications for crustal accretion at superfast spreading centers. *J. Geophys. Res.* 114, B03207. doi:10.1029/2007JB005436

Rabinowicz, M., and Briais, A. (2002). Temporal variations of the segmentation of slow to intermediate spreading mid-ocean ridges 2. A three-dimensional model in terms of lithosphere accretion and convection within the partially molten mantle beneath the ridge axis. *Journal of Geophysical Research* 107 (11), 979–1025. doi:10.1029/2001JB000343

Ribe, N., and Delattre, W. (1998). The dynamics of plume—ridge interaction—III. The effects of ridge migration. *Geophysical Journal International* 133, 511–518. doi:10.1046/j.1365-246X.1998.00476.x

Ribe, N. M. (1996). The dynamics of plume-ridge interaction: 2. Off-ridge plumes. *Journal of Geophysical Research-Solid Earth* 101, 16195–16204. doi:10.1029/96jb01187

Ribe, N. M., Christensen, U. R., and Theißing, J. (1995). The dynamics of plume-ridge interaction, 1: ridge-centered plumes. *Earth and Planetary Science Letters* 134, 155–168. doi:10.1016/0012-821X(95)00116-T

Rubin, K., Sinton, J., Maclennan, J., and Hellebrand, E. (2009). Magmatic filtering of mantle compositions at mid-ocean-ridge volcanoes. *Nature Geoscience* 2, 321–328. doi:10.1038/ngeo504

Rudge, J. F., Maclennan, J., and Stracke, A. (2013). The geochemical consequences of mixing melts from a heterogeneous mantle. *Geochimica et Cosmochimica Acta* 114, 112–143. doi:10.1016/j.gca.2013.03.042

Ryan, W. B. F., Carbotte, S. M., Coplan, J. O., O'Hara, S., Melkonian, A., Arko, R., et al. (2009). Global multi-resolution topography synthesis. *Geochemistry Geophysics Geosystems* 10, Q03014. doi:10.1029/2008GC002332

Salters, V., and Stracke, A. (2004). Composition of the depleted mantle. *Geochemistry Geophysics Geosystems* 5, Q05B07. doi:10.1029/2003gc000597

Sandwell, D. T., Winterer, E. L., Mammerickx, J., Duncan, R. A., Lynch, M. A., Levitt, D. A., et al. (1995). Evidence for diffuse extension of the Pacific Plate from Pukapuka ridges and cross-grain gravity lineations. *J. Geophys. Res.* 100, 15087–15099. doi:10.1029/95JB00156

Scheirer, D. S., Macdonald, K. C., Forsyth, D. W., and Shen, Y. (1996). Abundant seamounts of the Rano Rahi seamount field near the southern East Pacific rise, 15Δ S to 19Δ S. *Marine Geophysical Research* 18, 13–52. doi:10.1007/BF00286202

Schilling, J. (1973). Iceland mantle plume: geochemical study of Reykjanes Ridge. *Nature* 242, 565–571. doi:10.1038/242565a0

Schilling, J. (1991). Fluxes and excess temperatures of mantle plumes inferred from their interaction with migrating mid-ocean ridges. *Nature* 352, 397–403. doi:10.1038/352397a0

Schilling, J.-G. (1985). Upper mantle heterogeneities and dynamics. *Nature* 314, 62–67. doi:10.1038/314062a0

Schmerr, N., Garnero, E., and McNamara, A. (2010). Deep mantle plumes and convective upwelling beneath the Pacific Ocean. *Earth and Planetary Science Letters* 294, 143–151. doi:10.1016/j.epsl.2010.03.014

Schouten, H., Dick, H. J. B., and Klitgord, K. D. (1987). Migration of mid-ocean-ridge volcanic segments. *Nature* 326, 835–839. doi:10.1038/326835a0

Shorttle, O., Maclennan, J., and Jones, S. M. (2010). Control of the symmetry of plume-ridge interaction by spreading ridge geometry. *Geochemistry Geophysics Geosystems* 11, Q0AC05. doi:10.1029/2009GC002986

Shorttle, O., Rudge, J. F., Maclennan, J., and Rubin, K. H. (2016). A statistical description of concurrent mixing and crystallization during MORB differentiation: implications for trace element enrichment. *Journal of Petrology* 57, 2127–2162. doi:10.1093/petrology/egw056

Sleep, N. H. (1996). Lateral flow of hot plume material ponded at sublithospheric depths. *Journal of Geophysical Research Solid Earth* 101 (101), 28065–28083. doi:10.1029/96JB02463

Spulber, S. D., and Rutherford, M. J. (1983). The origin of rhyolite and plagiogranite in oceanic-crust - an experimental-study. *Journal of Petrology* 24, 1–25. doi:10.1093/petrology/24.1.1

Stoffers, P., Worthington, T., Hékinian, R., Petersen, S., Hannington, M., and Türkay, M. (2002). Silicic volcanism and hydrothermal activity documented at Pacific-Antarctic Ridge. *Eos, Transactions American Geophysical Union* 83, 301–304. doi:10.1029/2002EO000215

Stracke, A., and Bourdon, B. (2009). The importance of melt extraction for tracing mantle heterogeneity. *Geochimica et Cosmochimica Acta* 73, 218–238. doi:10.1016/j.gca.2008.10.015

Stracke, A., Genske, F., Berndt, J., and Koornneef, J. M. (2019). Ubiquitous ultra-depleted domains in Earth's mantle. *Nature Geoscience* 12, 851–855. doi:10.1038/s41561-019-0446-z

Stracke, A., Hofmann, A. W., and Hart, S. R. (2005). FOZO, HIMU, and the rest of the mantle zoo. *Geochemistry Geophysics Geosystems* 6, Q05007. doi:10.1029/2004GC000824

Stracke, A., Zindler, A., Salters, V., McKenzie, D., and Grönvold, K. (2003). The dynamics of melting beneath Theistareykir, northern Iceland. *Geochemistry Geophysics Geosystems* 4, 8513. doi:10.1029/2002gc000347

Stroncik, N. A., and Devey, C. W. (2011). Recycled gabbro signature in hotspot magmas unveiled by plume–ridge interactions. *Nature Geoscience* 4, 393–397. doi:10.1038/ngeo1121

Thirlwall, M. F. (1997). Pb isotopic and elemental evidence for OIB derivation from young HIMU mantle. *Chemical Geology* 139, 51–74. doi:10.1016/S0009-2541(97)00033-8

Todt, W., Cliff, R. A., Hanser, A., and Hofmann, A. W. (1984). "^{202}Pb + ^{205}Pb double spike for lead isotopic analyses," in *Terra cognita*. (Braunlage).

Todt, W., Cliff, R. A., Hanser, A., and Hofmann, A. W. (1996). "Evaluation of a 202Pb-205Pb double spike for high-precision lead isotope analysis," in *Geophysical monograph*. Editors S. Hart, and A. Basu (San Francisco: American Geophysical Union), 429–437.

Toomey, D. R., Wilcock, W. S. D., Conder, J. A., Forsyth, D. W., Blundy, J. D., Parmentier, E. M., et al. (2002). Asymmetric mantle dynamics in the MELT region of the East pacific rise. *Earth and Planetary Science Letters* 200, 287–295. doi:10.1016/S0012-821X(02)00655-6

Toplis, M. J., and Carroll, M. R. (1995). An experimental study of the influence of oxygen fugacity on Fe-Ti oxide stability, phase relations, and mineral—melt equilibria in ferro-basaltic systems. *Journal of Petrology* 36, 1137–1170. doi:10.1093/petrology/36.5.1137

VanderBeek, B. P., Toomey, D. R., Hooft, E. E. E., and Wilcock, W. S. D. (2016). Segmentation of mid-ocean ridges attributed to oblique mantle divergence. *Nature Geoscience* 9, 636–642. doi:10.1038/ngeo2745

White, W., Hofmann, A., and Puchelt, H. (1987). Isotope geochemistry of Pacific mid-ocean ridge basalt. *Journal of Geophysical Research* 92, 4881–4893. doi:10.1029/jb092ib06p04881

White, W., and Schilling, J. (1978). The nature and origin of geochemical variation in Mid-Atlantic Ridge basalts from the central North Atlantic. *Geochimica et Cosmochimica Acta* 42, 1501–1516. doi:10.1016/0016-7037(78)90021-2

Willbold, M., and Stracke, A. (2006). Trace element composition of mantle end-members: implications for recycling of oceanic and upper and lower continental crust. *Geochemistry Geophysics Geosystems* 7. doi:10.1029/2005GC001005

Yale, M. M., and Phipps Morgan, J. (1998). Asthenosphere flow model of hotspot–ridge interactions: a comparison of Iceland and Kerguelen. *Earth and Planetary Science Letters* 161, 45–56. doi:10.1016/S0012-821X(98)00136-8